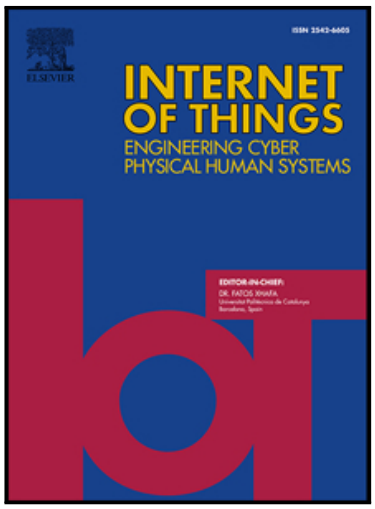

Lightweight Multi-Hop Routing Protocol for Resource Optimisation in Edge Computing Networks

Kennedy Chinedu Okafor , Bamidele Adebisi , Kelvin Anoh

PII: S2542-6605(23)00081-1
DOI: https://doi.org/10.1016/j.iot.2023.100758
Reference: IOT 100758

To appear in: *Internet of Things*

Received date: 21 February 2023
Revised date: 10 March 2023
Accepted date: 14 March 2023

Please cite this article as: Kennedy Chinedu Okafor , Bamidele Adebisi , Kelvin Anoh , Lightweight Multi-Hop Routing Protocol for Resource Optimisation in Edge Computing Networks, *Internet of Things* (2023), doi: https://doi.org/10.1016/j.iot.2023.100758

Optimisation in Edge Computing Networks

Kennedy Chinedu Okafor[1,2], Bamidele Adebisi[2] and Kelvin Anoh[3]
[1]Mechatronics Engineering, Federal University of Technology-Owerri, Nigeria
[2]School of Engineering, Manchester Metropolitan University, Manchester M1 5GD, UK;
[3]School of Engineering, University of Chichester, Bognor Regis, PO21 1HR, United Kingdom
k.okafor@mmu.ac.uk, b.adebisi@mmu.ac.uk, k.anoh@chi.ac.uk

Abstract— Data transmission over power line communication (PLC) infrastructure will proliferate lightweight Internet of Things (IoT) nodes in 5G and 6G networks. Consequently, a corresponding lightweight multi-hop routing protocol (LMRP) with reduced path loss and computational complexities will be required at the edges of PLC networks to connect the cloud sinks. Using a multi-layered system architecture, we present an LMRP for optimal routing and highlight the components of a smart PLC network comprising edge power pool orchestration, edge layer service provisioning, fog latency layer, and cloud resilient backbone. The LMRP reduces path loss and node failure states at the edge while optimising throughputs, minimum cost flow, and signal stability. A multi-hop deterministic testbed is designed and applied in three different locations to estimate path loss leveraging TelosB IoT node, Raspberry Pi (RPI) with NesC, and Java scripted logger application. Three different testbeds of varying path loss characteristics at the Federal University of Technology Owerri (FUTO) are used while the analysis was completed at Manchester Metropolitan University engineering LAB. The result of PL mitigation in Location 1 (sonic FUTO) shows 33.89%, 33.25%, and 32.77% with genetic algorithm (GA), particle swarm optimisation (PSO), and the proposed LMRP, respectively. In Location 2 (Old SEET Complex, FUTO), the PL obtained are 33.81%, 33.57%, and 32.62%, while Location 3 (New SEET Complex, FUTO) yields 33.65%, 33.41%, and 32.74% in PL mitigation for GA, PSO, and LMRP, respectively. Despite improved PL mitigation, the results also show that the proposed scheme offers a lightweight routing performance of at least 76.30% compared to similar schemes.

Keywords **— Driverless Cars, Edge Computing, Internet of Things, Lightweight Routing Optimisation, Multi-Hop Routing Protocol, Path Loss Optimisation.**

I. INTRODUCTION

Recent trends in smart infrastructure (e.g., driverless cars, smart grids, and several automated systems) show an increased need for power line communication (PLC) networks to transfer converged traffic (e.g., data, voice, and video). The PLC in IoT is standardised by ITU-T G.9903 to digitally route data over conventional electric power lines [1]. Although largely discussed in terms of other physical layer requirements, PLC networks require an efficient routing policy and minimised path loss incidents to achieve high-speed, dependable, secure, and bidirectional data communications. This is the major constraint to the development trends in smart grids [2] and several other cyber-physical applications, such as driverless smart transport systems [3].

Future connected grid networks have a lot of potential to utilise the Internet of Things (IoT)-enabled PLC systems. As an established, affordable, and reliable communication technology, PLC is now much more appealing for such networks because of new research efforts in the "In-band full-duplex (IBFD) broadband PLC (BB-PLC)" application [3]. IBFD can boost data throughput and spectrum efficiency in communication networks. Due to their lightweight characteristics on network resources, IoT devices are versatile and can be installed in various low-latency and high-throughput applications. IoT-PLC edge routing (ITU-T G.9903) is a pertinent technology standardised through IPV6 routing protocol for low-power and lossy networks (RPL RFC6550) [1]. Additionally, PLC technology is now advanced, affordable, dependable, and safe with this routing protocol [4]. According to their transmission frequencies, the narrow band PLC (NB-PLC) and the broadband PLC (BB-PLC) are two prominent PLC technologies. Both systems have difficulties when millions of devices transmit and receive data, and each one has a role in different setup scenarios and regulatory regimes [4]. The IoT-Lightweight PLC (IoT-LPLC) perfectly fits large networks and distant factories under optimised RPL. The RPL IPV6 is widely utilised in many fields, including the military, industry, smart cities, and smart buildings via outlet and switch ports. The reason for wide adoption is that it offers a straightforward method of utilising the same infrastructure seamlessly while addressing issues about data transmissions such as path loss, fault tolerance, security, energy usage, and load balancing [5]. This popular routing protocol for low-power and lossy networks has not yet been fully optimised for real-time adaption in cyber-physical systems [6]. For instance, using IoT-PLC integrated Layer 2 devices, the existing smart factory floor equipment must be controlled with a lightweight edge routing scheme [6]. Any edge node could be connected throughout the office building, providing stable communication between inside and outside of the building while connecting multiple nodes. Due to strong encryption and the flexibility of interconnecting and grouping devices, industry 4.0 will benefit significantly. IoT-LPLC is remarkably safe, dependable, and secure. This confers excellent market differentiation from past alternatives.

Additionally, the need for data speeds and network coverage is growing at the edge. The use of IBFD technology is one way to meet the growing need for data interchange in PLC networks [7], [8]. As demonstrated in these works, the IBFD technology could boost data speeds and reduce latency in BB-PLC. Also, it can extend network reachability by utilising full-duplex Fog relay nodes. Like most communication devices, a PLC channel has issues with spread-spectrum radio transmissions in a crowded setting [9]. Implementing IBFD for BB-PLC becomes challenging due to path loss constraints. There are several fundamental obstacles to IBFD technology. For instance, at 28GHz, signal path loss (PL) is prominent [10],[11]. Some propagation measurement studies demonstrate how mmWave attenuation is addressed while utilising the

available frequency resource in the 5G cellular networks [11]. According to [12], the performance of outdoor mmWave ad-hoc networks demonstrates that in the event of some PL blockages, mmWave may support high density and substantial spectral efficiency. Path loss could still provide a significant rate coverage challenge. The performance will be impaired without an adequate understanding of channel characteristics and lightweight routing schemes.

A major challenge with IBFD is that the edge computing technologies have failed to account for a robust lightweight routing scheme for real-time traffic provisioning while dealing with the issues of PL. The layer-three QoS metrics in legacy PLC network designs are severely constrained and cannot support massive traffic workloads due to serious interference and distortion issues within the PLC transceiver's channel block [13]. To address this issue, a resilient-oriented architecture of IoT-PLC clusters was proposed [9]. With a connection-oriented network, a reliable routing strategy will create full-duplex routes and carry out data offloading more efficiently.

From existing literature, various efforts have been made with the PLC fields to improve latency, throughput, path loss efficiency, energy drain, and other metrics within PLC ITU-T G.9903 routing at the edge network [4]. To date, there are initiatives to develop IPv6 routing protocols for lossy and low-power networks (LLNs) [1], [14], [15]. Several authors created protocols to suit devices with limited resources in commercial, domestic, and urban settings [16]. For instance, the authors [1], proposed emergency RPL (EMRPL), which can efficiently forecast the course of action and communicate sensory data in real-time. In [17], the authors proposed a PriNergy-RLP approach that reduces end-to-end delay, energy consumption, and overhead on mesh IoT networks without considering PL incidents. In [18], the authors looked at congestion and QoS-Aware RPL for IoT applications (CQARPL) and used a multi-metric evaluation for route conditions. The focus was on transmission and congestion control in IoT nodes. Most works on IPV6 RPL LLNs did not explore PL [19].

The interface between the IoT-PLC device and the edge-to-Fog network at the application layer handles data display and formatting. To distribute communication resources to nodes, the constrained application protocol (CoAP) was employed as a RESTful scheduling function [20]. Similarly, the authors [21] focused on Mobile IoT communication using message queuing transport telemetry (MQTT) protocol. The authors [22] concentrated on reliability-focused pub/sub messaging protocol, i.e., advanced message queuing protocol (AMQP) which was extended to serve as a communication interface for robotic technology (RT) middleware (RT-Middleware). The authors [23] presented a lightweight Xtensible message and presence protocol (XMPP) with publish/subscribe mechanism for resource constrained IoT devices. RESTful API has been used for web application integration and data tracking [24]. These lightweight algorithms are beneficial in cyber-physical applications but may suffer from PL challenges. Hence, further optimisation is needed at the edge.

Regarding edge communication optimisation, the work [25] proposed a multi-objective QoS optimisation routing in the industrial IoT domain. In [26], the authors proposed a unique algorithm for locating routing paths with the least amount of power loss while enhancing the optical signal-to-noise ratio of the routing paths. In [27], an artificial neural network (ANN), the multi-layer perceptron (MLP) neural network was used to precisely forecast PL. In [28], the authors focused on an exhaustive search algorithm (ESA) based on weighted least square (WLS) minimisation for network localisation. An algorithm for queen honeybee migration for routing and transmission paths was discussed [29]. Other routing and PL optimisation models were investigated, such as genetic algorithm (GA) [30], ant colony algorithm (ACA) [31], gravitational search algorithm [32], co-evolutionary optimisation algorithm (CEOA) [33], particle swarm optimisation (PSO) [34], whale optimisation (WO) [35] and flower pollination algorithm (FPA) [36]. The works in [37]-[40] contributed significantly to PL propagation and optimisation. But while various efforts came with great traffic provisioning, new challenges for the current PLC network have emerged with traffic routing and PL optimisation. But research on the multi-path lightweight routing of PLC networks is seldom reported.

Regarding the market, this article proposes a next-generation IoT-Lightweight PLC (IoT-LPLC) that significantly impacts the edge automation layer. It maximises performance and versatility, providing an edge over other legacy PLC solutions currently on the market. This study suggests a connection-oriented resilient routing approach for any edge computing system in a typical PLC network.

To prevent data stream distortion between adjacent nodes while sending high-speed data traffic, this article explores the principle of connection-oriented signalling. The proposed robust routing strategy specifies the robust weighted value of each connection.

Now, no RPL-based routing protocol exists for real-time efficient routing in cyber-physical edge networks. Chanel traffic signaling [41] and RPL protocols for connection-level QoS are largely missing especially for time-stamped CPS. As a result, it is possible to significantly enhance routing resilience in edge-distributed IoT-PLC architecture. This article seeks to fix the problems of reactive RPL (PLC ITU-T G.9903), and channel characteristics at the edge layers.

The main contributions of this paper include:

- For the PLC datastream routing policy, a novel SPLCN architecture is designed to optimise the *k*-shortest routing policy.
- For the edge layer, data transmission is proposed with a minimum cost flow problem to determine the best communication route that saves energy, reduces PL and computational complexity.
- Testbed characterisation of lightweight PL environment with optimisation validation involving GA and PSO respectively.
- Edge routing validation with lightweight application routing protocols such as REST, CoAP, MQTT, XMPP, and AMQP.

The remaining parts of this paper are organised as follows. Section II presents the baseline system model. Section

III reports the experimental path loss theory with other research efforts. Section IV discussed the experimental designs, radio models, and their significance at deployment sites. Section V presents results on PL mitigation, energy depletion, frequency comparisons, and optimisation evaluations. Section VI presents experimental validations while the work concludes in Section VII.

II. System Model

This study proposes an SPLCN architecture to support PL and routing optimisations. Figure 1 shows a 2×2 MIMO BBPLC with IBFD-enabled features. It has two modems interacting with one another simultaneously. Transceivers TRX1 and TRX3 are present in the first modem (local node), whereas TRX2 and TRX4 are present in the second modem (remote node). Signals sent by transmitters TX1 and TX3 of the local node are signals of interest (SI), whereas those sent by transmitters TX2 and TX4 of the remote node are SI at the edge layer.

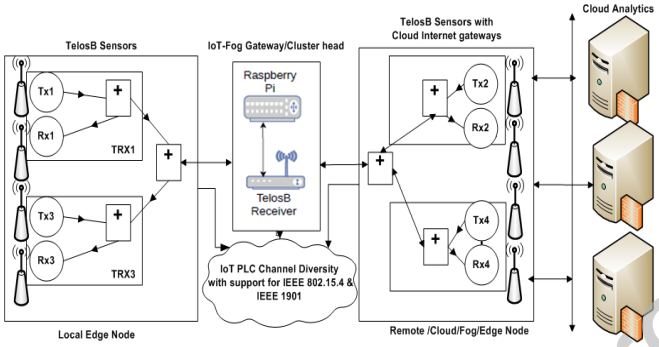

Figure 1: A redesigned 2×2 MIMO IBFD communication system for SPLCN architecture.

We represent the data received by j^{th} −receiver, which is typically in the time domain, as:

$$\gamma_j(t) = \sum_{i=0}^{n-1} L_i(t) * h_{ij}(t) + \omega_j(t) \quad (1)$$

where n is the default number of active transceivers, $L_i(t)$ is the lightweight signal of the i^{th} transmitter, $h_{ij}(t)$ is the channel impulse response from the connection between i^{th} transmitter and j^{th} receiver, and $\omega_j(t)$ represents the impulsive and white Gaussian noise captured at the j^{th} receiver. But at the edge layer, poor PLC channel characteristics and signal interference between edge nodes create a routing loop problem considering (1). Current multi-path routing methods are not suited for large BPLC networks, hence PLC ITU-T G.9903 routing was introduced in the validations. Also, PL must be significantly reduced for long-range payload delivery in Figure 2.

A. SPLCN Architecture

Distributed edge computing with lightweight processing and storage capabilities is used to enable local data processing in Figure 2 before applying the routing scheme. The fundamental concept behind the proposed connection-oriented routing strategy is that the routing calculation in the IoT-PLC network may be performed using the shortest path, thereby overcoming the limitations of (1).

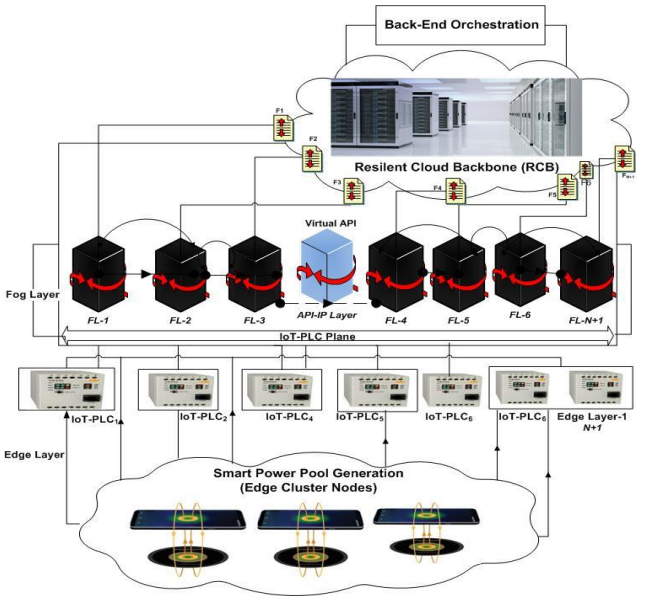

Figure 2: The proposed multi-layer SPLCN architecture shows four network layers from the edge devices to the cloud; the layers include the smart power pool isolation layer (SPPIL), the edge automation layer (EAL), the Fog latency layer (FLL), and the cloud core resilient layers (CCRL).

In addition, terminal nodes that work with edge computing resources will use the routing policy exchange signals. While the full-duplex route is operational in (1), new links can be constructed, and the related surrounding nodes use it to route to the upper layers. Initial route data can be disseminated around the edge network and stored on possible edge servers. When the service request is received, the closest edge node is selected as the edge data cluster head (EDCH). As the original data are resource intensive, they are processed at edge cluster heads and updated to the cloud data center.

Figure 2 shows the layered SPLCN architecture for a transparent routing scheme. Its main elements include the smart power pool isolation layer (SPPIL), the edge automation layer (EAL), the Fog latency layer (FLL), and the cloud core resilient layer (CCRL). The edge natives are a subset of the global grid cluster mapped into the Fog implementation layer of the SPLCN. The stream power pool (which provides energy-neutral IoT) is a fundamental advantage of lightweight IoT-PLC technology over other communication schemes. The FLL is used for latency reduction and resource maximisation during upward datastream offloading into the cloud.

Finally, the CCRL plays a very vital role in the entire architecture. In this case, the technique of anticipating potential disruptions to computational service offloading is known as cloud resilience. This offers service continuity and figures out the best recovery strategy without losing the network data. Cloud systems' resilience depicts their capacity to respond to failure while continuing to operate. Figure 2 shows the built cloud-native services running at the resilient cloud backbone (RCB). This is fault/failure tolerant for massive traffic workloads.

Here, we require to determine the most affordable way to transmit a specific amount of data across the edge-layered network in Figure 1.

In this context, constrained application protocol is required and maintains acceptable PL. This is useful for efficient data transmission. Since the IoT-PLC system requires performance considerations, lightweight MCFP can lower capacity restrictions for datastream flow provisioning. This is replaced by a demand condition or minimum routing [42]. The edge source is connected to a smart PLC adapter embedded in the distribution controllers in the implementation. This multi-hop functionality is shown in Figure 2.

At the layer 2 edge network, the powerline is reused to achieve data offload infrastructure needed for the distributed smart grid utility. In the design, the IoT-LPLC nodes are kept at rest to deliver data streams quickly and energy efficiently through cluster gateway having active communication links. Edge location sensor nodes (i.e., cluster heads) route data streams through labelled shortest-distance paths. Section II-C details the concept of minimum cost flow problem formulation (MCFPF). But this helps to route clustered nodes with time-varying link attributes (e.g., impulsive noise). It provides optimal path allocation and time-stamped links with auto-scaling. Hence, it is feasible to formulate a resilient routing algorithm that can optimise PL and still maintain reliability. The algorithm can support unicast, broadcast, and multicast transmission for converged traffic. These are useful for the overall computational efficiency and will improve routing concurrency in SPLCN.

B. Linear Node Distribution

The proposed system can be viewed as a directed graph $\mathcal{G} = \{V, E\}$ where V denotes the collection of vertices or nodes, $V = 1, \cdots, N$, and E denotes the collection of edges or links (connectivity of nodes). The edge Nodes at Layer 1 or cluster head sink node can be positioned inside or outside the monitored area, as shown in Figure 2.

In the case of a network with N linearly distributed nodes, a link $E(i,j)$ exists between nodes i and j with a Euclidean distance $d_{i,j}$, which must be less than the radio transmission radius $\Re$, i.e., $d_{i,j} < \Re$.

C. Minimum Cost Flow Problem Formulation (MCFPF)

Notations: For any IoT-PLC node $\gamma_j(t)$, an edge layer subnet-set is denoted by $\mathcal{G}(\Psi) = \{1, \cdots, a\}$ and the PL nodes set is denoted by $o = \{a+1, \cdots, N\}$. We let $L_w = \{1, \cdots, l_w, \cdots, \mathcal{L}_w\}$ where $\mathcal{L}_w$ represents the IoT-PLC wireless links and $\mathcal{L}_p = \{1, \cdots, l_p, \cdots, \mathcal{L}_p\}$ where $\mathcal{L}_p$ is the number of PL links. Here, $l_w \epsilon\, \mathcal{L}_w$ denotes the index for the l_w^{th} wireless broadband link and $l_p \epsilon \mathcal{L}_p$ denotes l_p^{th} PL link. In addition, $\mathcal{L} = \mathcal{L}_w \cup \mathcal{L}_p$ represents all hybrid networks. Radio channel matrix $\mathcal{L}$ connects node i transmitter to node j and is described via (i,j). The optimisation design for lightweight routing information is provided for deployment localisation at the edge layers.

Let $\mathcal{G} = (V, E)$ be an internally connected digraph for edge nodes in Figure 1:

- Upstream and lower stream capacity functions $b: E \to \Re$ and $c: E \to \Re$, respectively;
- overhead cost payload function $\gamma: E \to \Re$;
- Cluster demand function $d: V \to \Re$ with $\sum_{v \in V} d(v) = 0$.

The edge MCFP determination has a mapping $f: E \to \Re$ with minimal routing cost for $\gamma_j(t)$. Hence, the new formulation is given as:

$$j(t) = \gamma_j(t) + \sum_{i=1}^{n} q_{c,i} * \sum_{j=1}^{m_i} b_{i,j}^{z} \tag{2a}$$

Subject to:

$$b(e) \le f(e) \le c(e) \qquad \forall e \in E \tag{2b}$$

$$\sum_{e^+=v} f(e) - \sum_{e^-=v} f(e) = d(v) \;\; \forall v \in V \tag{2c}$$

Here, n represents an IoT-LPLC node port; $q_{c,i}$ depicts i^{th} node in the q^{th} cluster location; q depicts location of a strong reception map, z designates non-overlapping channels; m_i depicts j^{th} node port at the i^{th} IoT-LPLC node. Note that $j(t) \le l$ is a critical objective in which l depicts IoT-LPLC nodes placed in a defined location domain. (2b) represents the node cluster capacity restrictions, and (2c) represents the node cluster demand restrictions.

For short linear node broadcasts, a cut represents a partition $V = S \cup T$, and the capacity of the relay cluster head is given as

$$c(S,T) = \sum\nolimits_{e^- \in S, e^+ \in T} c(e) - \sum\nolimits_{e^+ \in S, e^- \in T} b(e) \tag{3}$$

where S is the IoT-PLC source, T is the IoT-PLC time stamp, $c(e)$ represents the IoT-PLC cluster head, and $b(e)$ represents IoT-PLC buffer overflow. In the formulation, the flow in an edge cluster is a map $f: E \to \Re$ meeting the resource demand constraints for all $v \in V$; again, if the capacity restrictions stand for all $e \in E$, this is now representing the cluster admissible flow. As a result, the MCFP requires a flow of minimum cost overhead to save the battery life of the IoT-PLC node. This is realised with k-node shortest path constructs.

D. $\mathcal{K}$-Node Shortest Path

This is very important in Figure 2, especially in dealing with reliability at both edge layer service provisioning and fog latency layers. As part of the PL mitigation, we are to find the shortest path between edge source s and destination Fog t using non-negative link weights, then the second shortest path, etc., up to the K^{th} shortest path. The Algorithm I describe the optimal $\mathcal{K}$ -shortest paths, i.e.., $\mathcal{K} = \{\mathcal{P}_1, \mathcal{P}_1, \mathcal{P}_1, \cdots, \mathcal{P}_k\}$.

In Algorithm I, the method finishes after finding the unique shortest path for $\mathcal{K}$ = 1. Otherwise, a complex technique is used to identify each of the shortest pathways after the initial one. To modify the set $\mathbb{x}$ of potential shortest paths. The process uses an auxiliary set $\mathcal{S}$ which is made up of pairs of the form $(\mathcal{Q}, v)$, where $\mathcal{Q}$ is a path from s to t and $v \epsilon\, \mathcal{Q}$. This is used to modify a cluster of potential shortest paths. In the algorithm, θ stands for the operator opposite concatenation $\oplus$. Additionally, sub $\mathcal{Q}(v,w)$ signifies the sub-path of $\mathcal{Q}$ from node v to node w.

The process modifies the set of potential paths $\mathbb{x}$ by adding the shortest path $\mathcal{P}$ to set $\mathcal{K}$ from the previous iteration. After doing this, it uses the function shortest ($\mathbb{x}$) to discover the shortest path in this set and adds it as the subsequent shortest path to set $\mathcal{K}$.

The next adjustment is made to Set $\mathbb{x}$. The unique pair of the form $(\mathcal{P}, w)$ in set $\mathcal{S}$ and the related deviation vertex w associated with path $\mathcal{P}$ are first found using the function *GetDeviationVertex* $(\mathcal{S}, \mathcal{P})$. Then, we consider all the subsequent vertices in the sub-path $sub_p(w,t)$ except for the destination *t.* These are referred to as deviation vertices. We identify the deviation path—also known as the shortest route—from each such vertex v to the destination t, and we combine it with the sub-path of $\mathcal{P}$, $sub_p(s,v)$, which begins in s and ends in v, to create path $\mathcal{Q}$ from s to t. Then set $\mathbb{x}$ receives Path $\mathcal{Q}$.

We must alter the graph using the function *DisableV erticesAndEdges* to ensure that path $\mathcal{Q}$ has not previously been formed before the Dijkstra algorithm is run. This function eliminates from graph $\mathcal{G}$ all vertices that make up the sequence $sub_p(s,v) \ominus v$, together with all edge incident to those vertices. Notably, this guarantees that the newly created path $\mathcal{Q}$ is straightforward. Additionally, we take away the edge extending from the vertex v towards the target (t) for each previously discovered shortest path $\mathcal{P}' \in \mathcal{K} \cup \{\mathcal{P}\}$. This has the property: $sub_p(s,v) = sub_{\mathcal{P}'}(s,v)$. When path $\mathcal{Q}$ has been determined for each deviation vertex v, pair $(\mathcal{Q}, v)$ is added to set $\mathcal{S}$.

Algorithm I. Lightweight Connection $\mathcal{K}$ −Shortest Path Algorithm

Procedure **LRAP** ( ) History of IoT-PLC route service provisioning; Signaling < *Rqs msg, Conf msg, Rel Msg.*

Procedure $\mathcal{K} - \mathbf{SP}(\mathcal{G}, s, t, \mathcal{K})$
$k := 1$;
$\mathcal{P} :=$ SPD$(\mathcal{G}, s, t)$;
$\mathcal{S} := \{(\mathcal{P}, s)\}$;
$\mathbb{x} := \{\mathcal{P}\}$;
$\mathcal{K} := \{\mathcal{P}\}$;

While $k < K$ and $\mathbb{x} \neq \emptyset$ ***do***
Begin
$\mathbb{x} := \mathbb{x}\{\backslash \mathcal{P}\}$
$w := GetDeviationVertex(s, \mathcal{P})$
for $v \in \langle sub_p(w,t) \ominus \{t\} \rangle$***do***
Set all flows in all node resource layers $(\ell \in \mathrm{L}) = 0$;
Begin
$\mathcal{G}' := DisableVerticesAndEdges(\mathcal{G}, s, v, \mathcal{K}, \mathcal{P})$
$\mathcal{Q} := sub_p(s,v) \oplus SPD(\mathcal{G}', v, t)$;
$\mathbb{x} := \mathbb{x} \cup \{\mathcal{Q}\}$;
$\mathcal{S} = \mathcal{S} \cup \{(\mathcal{Q}, v)\}$
end;
$\mathcal{P} := shortest\ (\mathbb{x})$;
$\mathcal{K} := \mathcal{K} \cup \{\mathcal{P}\}$;
$k := k + 1$
end;
end {procedure}

end return

E. Node Energy Problem Formulation

The edge power pool orchestration requires resource optimisation. Hence, it is feasible to convert battery lifetime into MCFPs. Assuming the initial energy is E_c, the lifetime of the node i during routing is given as

$$T_i = \frac{E_c}{\sum l_w \in O(i) \beta l_w (1+\alpha) \frac{t_{l_w}}{T}} \quad (4)$$

where βl_w is routing multistep transactions over the PL channel. l_w is $i \in \mathbb{W}$. $O(i)$ and $I(j)$ denote outgoing and incoming links at the IoT-PLC deployment edge network. The state vectors at k^{th} is given as $\overrightarrow{s(k)} = [\, S_{1,2}(k), \ldots \ldots S_{i,j}(k) - 1]^{T_i}$. Now, a lifetime of the network is given as

$$T_{net} = \min_{i \in \mathbb{W}} T_i \,. \quad (5)$$

The first objective is to maximise the IoT-PLC network life at the edge during the routing phases. Therefore, the network lifetime maximisation problem is formulated below as a mixed integer convex optimisation problem [43] in (6):

$$\min_{i \in \mathbb{W}} \frac{1}{T_{net}} \quad (6a)$$

$$s.t.\ \ T_{net} \leq \frac{E_c}{\sum l_w \in O(i) \beta l_w (1+\alpha) \frac{t_{l_w}}{T}} \ (i \in \mathbb{W}) \quad (6b)$$

$$C_l \cdot t_l \geq W_l \quad (6c)$$

$$W_l \geq 0 \quad (6d)$$

$$t_l \in \{0, \Delta, 2, \Delta, \cdots\} \quad (6e)$$

The variables $T_{net}, W_l, and\ t_l$ must be considered in the routing scheme concerning $\gamma_j(t)$. Δ is the weight interval for the computation of the variables in (6). The first inequality in (3) states that each IoT-PLC node's energy usage during routing must not be greater than the battery's capacity for the whole network lifetime. The maximum transmission power restriction for all links makes up the second inequality. The restriction ensures that the data transmission is completed in time *T*. The energy flow conservation for all nodes is in (5). If the integer restrictions on t_l are relaxed for this formulation, the optimisation challenge would be convex type. Section IV discussed the explicit radio model.

F. Node Link Problem Formulation

Apart from node energy Optimisation, creating an IoT-PLC node-link formulation is solved with mixed-integer programming (MIP). Only the edge variables are integer-constrained to depletion rates under an active state. This is the next step in the SPLCN design. Let's imagine a two-layer probe arranged into *N* layers. The *N*-layer design issue with link capacities y_e for the top layer (Layer 2) is considered. This intermediate demand is met at the downstream or lower layer (i.e., layers 1-2) using a lightweight routing flow that drains less energy. This results in the identification of the optimised layer link capacity, u_g. Assume for a moment that the bottom layers are joined by a new layer. Accordingly, the traffic demand intensity for replicated layer 1, (i.e., which must be routed to the next Fog layer), u_g becomes the link path of the present lower layer. This ultimately determines the link bandwidth data stream offloading. The next step in the process is to

continue making the basic observation (on-demand traffic) for a specific layer (downstream) to match the connection resource capacity required for the upstream layer. This can be seen in factory automation pyramids driving cyber-physical systems.

As a result, if an IoT-PLC edge link in layer ℓ is represented by e^{ℓ}, then its capacity, $y_{e^{\ell}}^{\ell}$, is sent to layer $(\ell-1)$ via aggregated flows as $x_{e^{\ell}p^{\ell-1}}^{\ell}$ .To identify the datastream edge device cluster capacities in layer $(\ell-1)$, we denoted this variable with $x_{e^{\ell-1}}^{\ell-1}$. This represents the designated redundant flows or traffic demand needed to test resilience in an active link.

There are two subscript elements introduced, *d* for demand and *e* for the link—with the datastream *N*-layer model, which assumes an upward orientation in SPLCN design. The Fog layer can be simply one layer above the higher one (or layer ℓ in the multi-layer case). As a result, layer ℓ has a demanding workload placed on it by layer $\ell+1$, which is a hypothetical layer. The location of the initial demand workload d is also known. Thus, we can deploy the demand layer as the layer $\ell+1$ immediately above the topmost Fog layer ℓ as it currently exists. Therefore, we can equally analyse the generic relationship $y_{e^{\ell+1}}^{\ell+1}$ and $y_{e^{\ell}}^{\ell}$ for an edge-to-Fog layer ℓ in place of the relationship between h_d and y_e. It should be noticed that for the top (demand) layer, we have $h_d = y_{e^{L+1}}^{L+1}$. Once the relationship between two neighboring layers has been established, the layer ℓ link-path indicator can be written as $\delta_{e^{\ell}\,e^{\ell+1}p^{\ell}}^{\ell}$.

Another way to look at this is to think of the "links" in layer $\ell+1$ as the constraints placed on the IoT-PLC nodes. The resource layer problem can then be thought of as $(\ell+1)$ layer design challenge. This would imply that the *N* resource layer problems presented in the design could be generalised within a complex-layered space. Finally, the lightweight multi-hop routing protocol (LMRP) is a multi-hop routing protocol for PLC that minimises routing paths in SPLCN. The LMRP aims to optimise resources according to:

$$\boldsymbol{Min}\quad \boldsymbol{F} = \sum_{\ell=1}^{L}\sum_{e^{\ell}} \xi_{e^{\ell}}^{\ell}\, y_{e^{\ell}}^{\ell} \tag{7a}$$

Subject to:

$$\left(\sum_{\ell>0} p^{\ell} x_{e^{\ell+1}p^{\ell}}^{\ell} = y_{e^{\ell+1}}^{\ell+1}\right) \tag{7b}$$

$$\left(\sum_{\ell>0} p^{\ell}\delta_{e^{\ell}\,e^{\ell+1}p^{\ell}}^{\ell}\, x_{e^{\ell+1}p^{\ell}}^{\ell} = y_{e^{\ell}}^{\ell}\right) \tag{7c}$$

Where ***F*** denotes overall efficiency covering sets of nodes, overhead cost vector, clusters, PL channels resource provisioning.

As previously shown in [43], single-layer and two-layer IoT-PLC sensor arrays can have the shortest-path allocation rule applied for $\ell = 1 \cdots \infty$. Therefore, the lightweight resource allocation policy (LRAP) for the general multi-layer case in Figure 2 is shown with Algorithm I. In its structure, it could be noticed that $\zeta^{\ell} = (\zeta_1^{\ell}, \zeta_2^{\ell}, \ldots, \zeta_{E^{\ell}}^{\ell})$ depicts the vector representing the accumulated costs of the entire layered linkages ℓ $(\ell = 1, 2, \ldots, L)$. Considering only the layer-specific overhead, $\xi_{e^{\ell}}^{\ell}$ of link e^{ℓ} while reducing the link cost of IoT-PLC node clusters below ℓ, the function length_shortest_path $(e^{\ell+1}, \zeta^{\ell})$ returns the total shortest path on the routing list of the link $e^{\ell+1}$.

From Line 1, the routing scheme commenced with the nodes first powered by an edge stream power pool that charges the battery. This then provides depletable energy communication from the nodes to the cluster heads. The link state layers are then established from the edge to the fog while allowing the cloud resilient layer to orchestrate datastream. Auto-scaling based on resource availability is realised. The traffic request message, confirm message and release message designates the three different categories of signaling messages during routing. Routing computation is done by Dijkstra's shortest path and reliability degree value during active operation. This sorts every link according to its availability, chooses the best link, and adds it to the available topology. The route computation is then finished after getting the route result. To get the route result and the list of involved nodes, the resilient routing calculation is carried out.

Algorithm II. Lightweight connection-oriented Policy

Procedure **LRAP** () History of IoT-PLC RPL service provisioning; Signaling < Rqs msg, Conf msg, Rel Msg;

Begin
Func G.9903 ( );
Instantiate smart power pool for entire edge nodes ( );
Set all flows in all node resource layers $(\ell \in \mathrm{L}) = 0$;
Set $\zeta_{\mathrm{e}^1}^1 = \xi_{\mathrm{e}^1}^1$ for all links e^1 of layer 1.
for $\ell \coloneqq 1$ to $\mathrm{L}-1$ **do**
  for $\mathrm{e}^{\ell+1} \coloneqq 1$ **to** $\mathrm{E}^{\ell+1}$ **do** $\zeta_{\mathrm{e}^{\ell+1}}^{\ell+1}$
$\coloneqq \mathrm{length}\mathrm{h}_{\mathrm{shortest}}\mathrm{path}\left(\mathrm{e}^{\ell+1}, \zeta^{\ell}\right) + \xi_{\mathrm{e}^{\ell+1}}^{\ell+1}$;
for $\ell \coloneqq \mathrm{L}$ **down to** 1 **do**
  Begin
    for $\mathrm{e}^{\ell+1} \coloneqq 1$ **to** $\mathrm{E}^{\ell+1}$**do**
    Begin
      $\mathrm{p}(\mathrm{e}^{\ell+1}, \ell) \coloneqq \mathrm{length}_{\mathrm{shortest}}\mathrm{path}\left(\mathrm{e}^{\ell+1}, \zeta^{\ell}\right)$;
      $\mathrm{x}_{\mathrm{e}^{\ell+1},\mathrm{p}(\mathrm{e}^{\ell+1},\ell)\coloneqq \mathrm{y}_{\mathrm{e}^{\ell+1}}^{\ell+1}}^{\ell}$
    end.
for $\mathrm{e}^{\ell} \coloneqq 1$ **to** E^{ℓ} **do** $\mathrm{y}_{\mathrm{e}^{\ell}}^{\ell} \coloneqq \sum_{\mathrm{e}^{\ell+1}} \delta_{\mathrm{e}^{\ell}\,\mathrm{e}^{\ell+1}\,\mathrm{p}(\mathrm{e}^{\ell+1},\ell)}^{\ell}\, \mathrm{y}_{\mathrm{e}^{\ell+1}}^{\ell+1}$
call signalling ( );
construct battery sub-model output matrix ( );
if scaling Parameter ≔ Impulsive noise Aware
 then
 call Middleton Class-A ( );
Else
end
end {procedure}
if scalingParameterType is $\mathrm{length}_{\mathrm{shortest}}\mathrm{path}$ -Aware **then**
  parameterStatus←Predictor (history of Response Time)
Elseif scalingParameterType is Resource-Aware **then**
  parameterStatus←Predictor (history of QoS parameterStatus)
end if

If parameterStatus is higher than power-poolScale Up routing threshold **then**
  decision←Scale Up
Elseif parameterStatus is lower than power-poolScale Down threshold **then**
  decision←Scale Down routing
end if
end if
end return

The resilient routing computation is employed to provide the algorithm result and the list of participating nodes. The major problem is that resilient routing computational complexity must be implemented and compared with other RPL schemes. The reliability requires two multiple operations, with O-level complexity (1). For the dependability routing service in IoT-PLC networks, the complexity is only $O(n)O$ (1) when the number of complex network nodes approaches n.

As an important edge communication metric, the PL in IoT-PLC interfaces is further investigated for outdoor deployments. In this use case, the electromagnetic wave propagation in IoT-PLC wireless channel is represented as a power law function with a separation between the RF transmitter and receiver. The free space model and the two-ray model are considered. When there is a direct, unimpeded line of sight (LoS) between the transmitter and receiver, the received signal strength is predicted using free space propagation.

Given that the free space power received by an IoT-PLC receiver radio is d miles away from transmitting edge-node. As shown in Figure 1, PL is the difference (in dB) between the effective transmitted power and the received power during the routing operation. This is used to depict signal attenuation as a positive number measured in dB. In this context, the following equations illustrate the influence of node antenna gain [44].

$$P_r(d) = \left[\frac{P_t G_t G_r \lambda^2}{(4\pi)^2 d^2 L}\right] \quad (8)$$

where $\mathrm{P_t}$ = IoT transmitted power, $\mathrm{P_r}$ = IoT received power and $\mathrm{P_r(d)}$ =received power, which depends on the T-R (transmitter-receiver) spacing distance d.

$\mathrm{G_t}$ = transmitter antenna gain, $\mathrm{G_r}$ = receiver antenna gain, L = non-propagation-related system loss factor, $\mathrm{L} \geq 1$ and λ = Wavelength (m).

G_t and G_r are dimensionless quantities, however the values of P_r and P_t are in the same unit. The IoT-PLC RF, and filter losses as well as the transmission space diversity generate signal losses $L(L > 1)$. The received power diminishes with the square of the $T - R$ separation distance, according to the free space (1). This suggests that the received power decreases by 20 dB/decade as a function of distance. During the experiment in Section IV, the transmitted power P_t is obtained. But the PL measurements are calculated using (9a).

$$\mathrm{P_r(dBm)} = \mathrm{P_t(dBm)} - \mathrm{P_L(dB)} \quad (9a)$$

$$\mathrm{P_L(dB)} = 10\log\left[\frac{\mathrm{G_t G_r \lambda^2}}{(4\pi)^2 \mathrm{d^2}}\right] \quad (9b)$$

$$\mathrm{P_L(dB)} = -10\log\left[\frac{\lambda^2}{(4\pi)^2 \mathrm{d^2}}\right] \quad (9c)$$

By substituting (8) into (9a), this gives (9b). The free space model can accurately estimate P_r only for d values that are in the transmitting antenna's far field. (9d) can be obtained by simplifying (9c). To obtain the free space PL formula, we obtain (9d).

$$P_L = 20\log_{10}(4\pi) + 20\log_{10}(d) - 20\log_{10}(\lambda) \quad (9d)$$

If we put $\lambda(km) = {}^{0.3}/_{f(MHz)}$ into (9d), and simplify further, we have (9e).

$$P_L(dB) = 3.25 + 20\log_{10}(d) + 20\log_{10}(f) \quad (9e)$$

In the experimental testbed, 1m is used as the received power reference $P_r(d)$ in the close-range measurement. At any distance $d > d_0$, the received power, $P_r(d)$, is related to $P_r\ at\ d_0$. In the radio setup domain, the value $P_r(d_0)$ was determined by averaging the received power P_r at numerous locations d_0 away from the transmitter. Given that the received power P_r was obtained during the experiment and the transmitted power P_t obtained, path loss measurements (PLMs) were calculated using (8).

From (8), the experiment's P_t value was set $0dBm$, such that $P_r$in free space at a distance $d > d_0$ is then given by (10).

$$\mathrm{P_r(d)} = \mathrm{P_r\,(d_0)}\left(\frac{\mathrm{d_0}}{\mathrm{d}}\right)^2 \quad (10)$$

At high values of d, the P_r and PL in the two-ray model becomes frequency independent. In terms of dB, the PL for the two-ray model is given as (11).

$$\mathrm{P_L(dB)} = 40\log \mathrm{d} - (10\log \mathrm{G_t} + 10\log \mathrm{G_r} + 20\log \mathrm{h_t} + 20\log \mathrm{h_r} \quad (11)$$

By calculating the received signal intensity as a function of distance, PL can be used to forecast other channel parameters. Equ. (12) uses a route loss exponent, n, to express the average PL for each transmitter-receiver separation distance d.

$$P_L(d) \propto \left(\frac{d}{d_0}\right)^n \quad (12)$$

$$P_L(dB) = P_L(d_0) + 10nlog\left(\frac{d}{d_0}\right) \quad (13)$$

Where the average PL between the sender and receiver is measured in dB. $P_L(d_0)$ denotes referenced PL model (dB). When the d between the receiver and transmitter is at reference d_0, With d_0, as the close-in reference distance d_0, we can calculate the PL exponent, n from measurements taken close to the transmitter. This represents the rate at which the PL rises with distance d which gives T-R separation.

The edge network propagation environment has specific characteristics that affect the value of n. For instance, n = 2 in free space; nevertheless, n will increase in value in the presence of impediments. The free space PL formula is used to compute the reference PL (13).

Now, the estimated PL is calculated using (14), where n can be manually calculated or obtained with a linear regression analysis approach:

$$n = \frac{P_L(d) - P_L(d_0)}{10\log_{10}({}^{d}/_{d_0})}. \quad (14)$$

By reducing the gap between the observed data and the anticipated PL value of (13), the PL exponent can be

calculated from the measured data using LR. The PL exponent is given by (15a):

$$E(n) = \{P_{Lm} - P_{Lp}\}^2 \quad (15a)$$

where P_{Lp} is the experimental PL at d using (136). P_{Lm} is the measured PL at distance d in dB. The model (14) is obtained when (13) is substituted for P_{Lp} in (158). The PL exponent is then given by (14)

$$E(n) = \sum_{i=1}^{k}[P_{Lm} - P_L(d_0] - 10n\,Log10(\tfrac{d}{d_0})^2 \quad (15a)$$

By differentiating (15a), this gives

$$\frac{\partial E(n)}{\partial n} = -20n\log_{10}\left(\frac{d}{d_o}\right)\sum_{i=1}^{k}[P_{Lm} - P_L(d_0] - 10n\,Log10\left(\frac{d}{d_0}\right) \quad (15b)$$

Let $\frac{\partial E(n)}{\partial n} = 0$ and equate both the left-hand side and right-hand side, this implied that $-20n\log_{10}\left(\frac{d}{d_o}\right)$ yields:

$$\sum_{i=1}^{k}[P_{Lm} - P_L(d_0)] - \sum_{i=1}^{k} 10nlog10\left(\frac{d}{d_0}\right) = 0 \quad (15c)$$

Making n the subject in (15c) yields the PL exponent n:

$$n = \frac{\sum_{i=1}^{k}[P_{Lm} - P_L(d_0]}{\sum_{i=1}^{k} 10nlog10\left(\frac{d}{d_0}\right)} \quad (16)$$

With MATLAB scripts, n was computed (16).

$$P_L(dB) = P_L(d_0) + 10nlog10\left(\frac{d}{d_0}\right) + X_\sigma \quad (17)$$

Where X_σ is a zero-mean, Gaussian-distributed random variable with a standard deviation of σ; both values are in decibels. σ is computed with (16) to yield (18).

$$\sigma(dB) = \sqrt{\sum_{i=1}^{k}\frac{\left(P_{Lm} - P_{Lp}\right)^2}{N}} \quad (18)$$

Where P_{Lm} = experimental PL (dB)

P_{Lp} = predicted PL (dB)

N = No of data points = 25; σ = 2.3; $P_L(d_0) = 43.83$

These values were computed with MATLAB [45] for the derived PL model.

Now, by substituting these values in (17), this gives outdoor PL with IoT-PLC TelosB in (7).

$$P_L(dB) = 43.83 + 10(2.67)\log\left(\frac{d}{d_0}\right) + 2.3 \quad (1913)$$

$$P_L(d) = 43.83 + 10(2.67)\log\left(\frac{d}{d_0}\right) \quad (20)$$

The PL in (20) represents the PL model for any random distance d from the transmitter as the outdoor scenario for TelosB. The average PL of the indoor environment was determined using (9a). This is done with the transmitted power set at 0dBm and the received power measured at various distances from 10 to 60m at intervals of 1m. The determined average PL of the indoor environment for the TelosB nodes is later discussed in section IV.

III. Radio Energy Model

Consider the edge node cluster comprising N IoT nodes $\{S_1, \cdots, S_n\}$ used in Figure 2. The nearest IoT node to the edge network S_n and the farthest is S_1. During the multi-hop transmission of data, S_1 sends its data to the cluster head and the sink seamlessly. The transmission power influences the node transmission range. Therefore, the nodes are linearly placed from source to sink with their respective distances $\{d_1, d_2, \cdots, d_n\}$. The edge-to-Fog distance d is given by

$$d = \sum_{i=1}^{N} d_i\ . \quad (21)$$

The necessary transmission of one way to model energy is given as

$$E_t(\mu, d) = \mu(\lambda_t + \xi d^n) \quad (22)$$

Additionally, the receiver's energy usage for the same bitstream given as

$E_t(\mu) = \mu\lambda_r$

where μ = No of bits, λ_t and λ_r = Energy/bit consumed in the Tx and Rx, respectively.

d = distance

n = Path loss exponent (for perfect LoS between the transmitter and receiver, $n = 2$; n= 4 in dense urban locations)

$\lambda_t = \lambda_r = \lambda_e$

λ_e = Electronics Energy

(23a) and (23b) are obtained from (22) considering the crossover distance (i.e. approximately 87.6m).

$$E_t(d) = \{\mu\lambda_e + \mu\xi_{fs}d^2\} \quad if\ d < d_q \quad (23a)$$

$$E_t(d) = \{\mu\lambda_e + \mu\xi_{mg}d^4\} \quad if\ d \geq d_q \quad (23b)$$

The authority to route or distribute this message is

$$E_f(\mu, d) = E_e(\mu, d) + E_e(\mu) \quad (24)$$

$$E_f = 2\mu\lambda_e + \mu\xi_{fs}d^2 \qquad d < d_q \quad (25a)$$

Or

$$E_f = 2\mu\lambda_e + \mu\xi_{mp}d^4 \quad if\ d \geq d_q \quad (25b)$$

where

d_q = threshold distance is given as

$$d_q = \sqrt{\frac{\xi_{fs}}{\xi_{mp}}} \quad (26)$$

According to the experiment, the PL exponents for the indoor and outdoor testbeds, respectively, were calculated to be 2.67 and 2.77. Thus, using (23a) and (23b) respectively, we now provide the amount of energy used by the IoT transmitter to power the radio electronics and the amplifier for outdoor and inside use.

$$E_t(d) = \{\mu\lambda_e + \mu\xi_{fs}d^{2.67}\} \quad (24a)$$

$$E_t(d) = \{\mu\lambda_e + \mu\xi_{fs}d^{2.77}\} \quad (24b)$$

Using the determined PL, the energy required to transmit the message can be given as

$$E_f = 2\mu\lambda_e + \mu\xi_{fs}d^{2.67} \quad (25a)$$

$$E_f = 2\mu\lambda_e + \mu\xi_{fs}d^{2.77} \quad (25b)$$

The edge source IoT node will transmit *j* bits data stream to the distant sink node through direct or multi-top transmission when it detects an event. The *N*-hop transmission is explored from source to sink node because multi-hop transmission is more energy efficient when *d* is large. For each node to use the least amount of energy at the same pace, we must determine the ideal multi-hop number and each distance *d*. The total energy required to transmit one bit of data ($\mu = 1$) over an *N*-hop route will be calculated using (26) and (27).

$$E_N = \sum_{i=1}^{N}(\lambda_e + \xi d_1^n) + \sum_{i=2}^{N}\lambda_e \quad (26)$$

$$E_N = \lambda_e + \xi d_1^n + \sum_{i=1}^{N}(2\lambda_e + \xi d_1^n) \quad (27)$$

Where $\xi = \xi_{fs}$ when $n = 2$ and $\xi = \xi_{mp}$ when $n = 4$

$$E_N = (2N-1)\lambda_e + \sum_{i=1}^{N}\xi d_1^n \quad (28)$$

For the same distance between nodes $\sum_{i=1}^{N} d_i = d$, $\sum_{i=1}^{N} d_i$ in (15) has an optimised value if $d_1 = d_2 = \cdots . d_n = {}^{H}/_{n} . H$ is the deployment length. Then E_N is then equal to

$$E_N = (2N-1)\lambda_e + \xi N^{1-n} d^n \quad (29)$$

Then (29) is the minimum when $E_N = 0$.

Since the distance d_i and traffic length is the same for all sensor nodes, the sensor nodes consume energy at the same rate. Hence, $\lambda_1 \approx \lambda_2 \approx \lambda_3 \approx \lambda_N$

The radio parameters are given as λ_e =50nJ/bit, $\xi_{fs} = 10pJ/bit/m^2$ $E_0 = 0.5J, \xi_{mp} = 0.0013pJ/bit/m^4$ and 16 bytes. If these values are inserted into (24a) and (24b), the energy consumed for transmission and reception of data for various distances used in the experiment was calculated.

The ideal number of IoT $S(\geq S_{min}$, the transmission distance d_i, and the corresponding power level $P(d_i)$, for each sensor node $S_i(i = 1, \cdots . N)$ such that the energy consumption of the sensor nodes is equal or that the sensor nodes deplete their energy at the same rate (30). This must be determined to achieve the maximum lifetime of the sensor nodes.

Finding S_i and d_i that reduces the energy consumed by each sensor node is the goal.

$$Min\{\lambda_1 \approx \lambda_2 \approx \lambda_3 \approx \lambda_N \quad (31a)$$

Subject to

$$d_i \leq R_{max} \quad (31b)$$

$$\sum_{i=1}^{n} d_i \geq H \quad (31c)$$

where the first condition (31b) identifies each node's transmission limit and the second (31c) guarantees that the nodes can cover the infrastructure locations under consideration.

In (31a), (31b), and (31c), we assume that the sensor nodes being examined have w distinct power levels, denoted by $(P_i, R_i), (P_w, R_w)$, where P_i is the power level at which sensor nodes communicate; R_i is the transmission range. The maximum transmission range is restricted to being $(R_{max} = R_w)$ the maximum transmission power level $P_{max} = P_w$. Like this, the sensor nodes can broadcast data up to a range of $R_{min} = R_1$ at the minimal power level $P_{min} = P_1$. It could be deduced that PL decreases as the transmission power rises. Also, there is a relationship between PL and the square of the signal frequency transmitter–receiver distance. The PL affects the degree of received power. With less received power, this will mean more PL is evidenced. To increase the power level available at the node receiver, efforts are then made to minimise PL using high-gain IoT devices with lightweight routing optimisation.

IV. Experimental Design and Analysis

A. Testbed Setup

In this section, a low-cost, and resource optimised TelosB IoT platform [45] with Raspberry Pi [46] is deployed. These are portable open-source hardware for various field experiments with test parameters [13]. As a deterministic testbed, the TelosB IoT platform is driven by the MSP430 CPU core and CC2420-ITU-T G.9903 instead of compatible RF interfaces. Similar experiments were described [46], [47] but lacked PL Optimisation contributions. In both indoor and outdoor location settings, this study focused on the PL, and battery depletion efficiency of edge-to-CH data stream transmission-offloading. Since Raspberry Pi (RPI), is not G.9903 compatible by default, the TelosB USB port is connected directly to the RPI module as shown in Figure 1. Keep in mind that the RPI has an ARM configuration, a quad-core CPU running at 1.2 GHz, a RAM size of 1GB, and a Linux OS. A Fog layer is used to store data streams from TelosB-based IoT devices in the Fog gateway. RPI offered a lightweight platform for TinyOS which supports the pass-through for Fog over the Internet (FoI) and hence designated as the sink data logger in Figure 3. It can also run an edge instance locally.

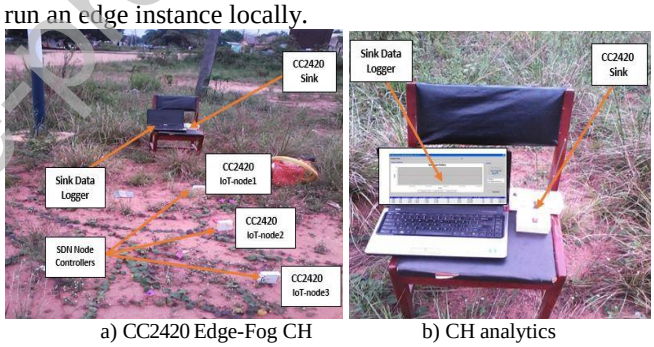

a) CC2420 Edge-Fog CH b) CH analytics

Figure 3. An experimental outdoor testbed for edge-Fog PL investigations.

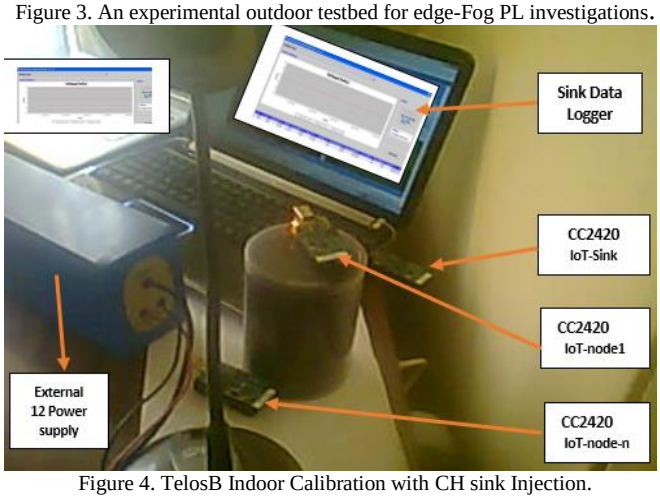

Figure 4. TelosB Indoor Calibration with CH sink Injection.

B. System Operating Kernel

As shown in Figure 3, the TelosB device has 10Kbyte RAM with 48Kbyte flash memory. Hence, the OS for IoT devices has a minimal memory footprint. Due to these limitations, general-purpose OS is not supported by the TelosB platform. Therefore, the TelosB transceivers coupled to the RPI module are controlled by the IoT software platform called TinyOS [48].

C. Software Framework Integration

NesC and Java are the two programming languages used to configure the CC2420 TelosB IoT nodes. The readings from the nodes were directly converted to values using NesC programs. The source codes were executed on TinyOS 2.*x*. For the MSP430 platform, TinyOS 2.*x* provides Java 1.5 cross-compilers and tools that are connected to TinyOS/NesC. The mote's USB port was used to compile and load the TinyOS code. For the compilation procedures, four files were created: the Make file, the Header file, the Configuration file, and the module file. In the testbed experiment, the nodes are set up to send data every 5 seconds, and when the message is sent successfully, the radio is turned off to save power. Most conversions for the typical measurement data are also encoded into the nodes, and the software has their readings set to SI units.

Following that, a Java graphic user interface was created and utilised for data collection in Figure 5. The application shows the data as it is sent and presents a graphical representation of the relationships between the sensor nodes for voltage, temperature, light intensity, and humidity [47]. PL was derived from the received signal strength datasets. Options to save data, clear data, start monitoring, and stop monitoring are available on the graphical display. Data supplied every 5 seconds up to 2 minutes was saved and maintained. The work averaged the saved data, which included up to 1000 separate counts. The datasets for the listed parameters were obtained for six weeks, with daily readings from 6 am morning to 6 pm.

With the node integration, the software composition largely adheres to the spine-leaf architecture highlighted in Figure 2. Data stream dissemination is made possible by software components using the two primary communication protocols. The forwarding of transmitted data streams (TX) is achieved with the layer 3 Internet Protocol (IP V6) design between the edge-Fog layer and the RPI controller located powering the Internet. Meanwhile, ITU-T G.9903 sets up seamless communication between TelosB nodes transmitting the edge data streams (TXs) to the controller RPI. On the RPI, the TinyOS mines data locally while serving as the raw data gathering environment with TelosB nodes. The RPI data collection repository is shown in Figure 4. Since the channel capacity of IEEE 802.15.4 is not compatible, G.9903 is then explored.

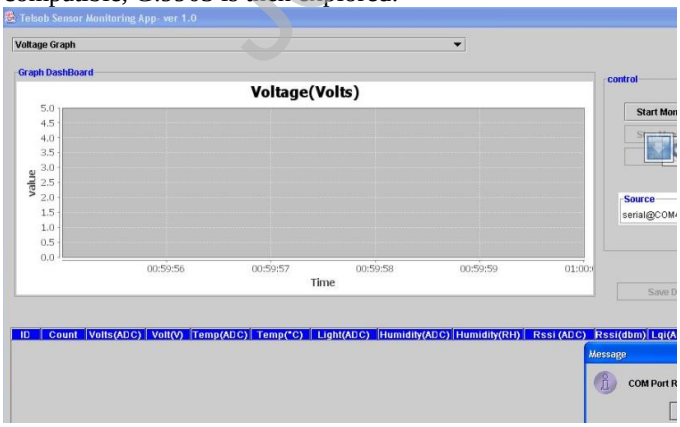

Figure 5. TelosB Virtua Machine JAVA GUI instance with no readings.

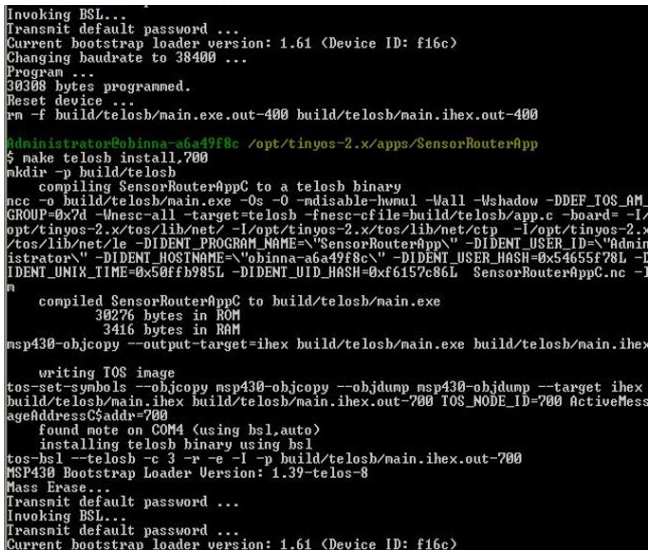

Figure 6. TelosB Virtua Machine TinyOS instance (Upstate).

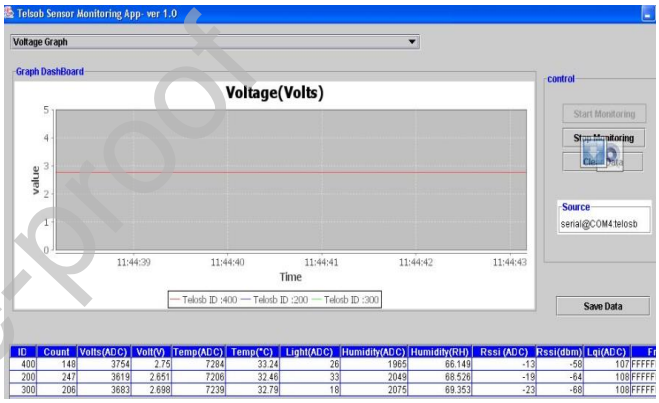

Figure 7. TelosB Virtual Machine JAVA GUI instance with readings.

The edge-Fog TX is put together by the Fog container wallet, which is implemented as a TinyOS image. This collects PL data from the edge sensors. Security functions are used by the Fog container wallet engine to assemble the edge-Fog TX. The SHA3-256 [46] provides cryptographic digests, while SHA3-256 delivers 256-byte-long transaction signatures. Because SHA3-256 is a quick and resource-conserving cryptographic primitive, its use is acceptable. Only one TelosB Sensor node at a time is used to send edge-Fog TXs on the testbed for this study which is powered by AA batteries (3.3v). Using channel 26 (2.4 GHz) and the TinyOS mac channel access mechanism, the TelosB device transmits data at a bandwidth of 250 kbit/s [46]. TelosB uses the CC2420 Transceiver chip, which complies with 802.15.4 [46]. This configuration also sets the CC2420's default transmission power to 0 dBm. Also, Line-of-Sight (LOS) and Non-Line of Sight (NLOS) are two experimental configurations that used indoor and out PL measurements respectively. Each edge node has a customisable ID with signed data packets. Also, each data size weighs 20 Bytes. If the expected ACK is absent, a packet is sent up to ten times again.

The evaluation of the edge-Fog TX technique looked at the transmission performance based on the volume of traffic expressed in bytes and the number of packets delivered, including retransmissions. In the LOS scenario, the packet overhead, or the percentage of extra packets transmitted on top of data packets, is always around 100%, whereas greater

packet values are observed in the NLOS situation owing to retransmissions. The result of ACK messages verifying each packet sent is this significant packet overhead. The TelosB-RPI platform may function for roughly 10 years if the deep inactive current is less than 0A, has two AA batteries with 1,200mWh each; and wakes up once/day for measurements. A traffic volume that is around 10 times the size of the data block is seen when a TX is made up entirely of payloads.
We observed that energy efficiency rises when more data streams are contained within a single TX, per energy usage measurements. This overhead is added by TinyOS because of the costly calculations needed. Therefore, it is desirable to send multiple data streams; each signed with a TelosB signature. Since the node uses less energy, this platform's energy efficiency is slightly lower than the results reported in [47].

V. RESULT ANALYSIS

In this section, the results from the edge network PL studies and lightweight routing validations are presented. The relevance of this section is to enable the construction of reliable IoT PLC edge networks. This is by understanding the impact energy drain of a wave propagating between the transmitter and the receiver, under the routing scheme.

A. Path Loss Mitigation Analysis

The theoretical models in Section In Table 1, the TelosB node characterisation of the outdoor empirical measurement environment was determined using (1). The transmitted power was set at 0 dBm while the received power was measured at various distances from 10 to 60m at intervals of 10m. The calculated average PL in the outdoor setting is shown in Table 1.

Table 1. average outdoor environment PL for IoT TelosB nodes.

Distance	Avg. P_L (dB) Node 1	Avg. P_L (dB) Node 2	Avg. P_L (dB) Node 3	Avg. P_L (dB) Node 4
1	40.7	46.0	44.8	43.83
5	61.4	64.1	62.3	62.60
10	68.1	69.6	65.8	67.83
15	82.4	75.9	74.7	77.67
20	80.3	77.7	81.9	79.97
25	77.6	88.5	81.3	82.47
30	81.5	88.5	89.5	86.50
35	88.7	89.2	84.7	87.53
40	75.8	88.2	86.3	83.40
45	82.3	91.8	85.5	86.53
50	84.7	91.8	92.2	89.57
55	78.8	88.8	89.3	85.63
60	92.2	92.43	92.3	92.3

Under multi-hub routing, numerous factors, including free-space loss, refraction, diffraction, reflection, aperture-medium coupling loss, and absorption, contributed to PL experienced in Figures 8, 9, and 10. Along with topographical contours, environment (e.g., urban/rural, vegetation, and foliage), propagation medium (dry or moist air), the distance between transmitter and receiver, and antenna height and placement, PL was influenced by these factors too. However, the PL estimation is better compared with [49], and [50] in free space using the deterministic approach. The proposed technique relies on the correct and thorough description of every item in the propagation space, including buildings, roofs, windows, doors, and walls, and is predicted to yield more accurate and trustworthy forecasts of the PL than the empirical techniques as shown in Figure 9. This observation will be useful for short propagation paths in connected vehicular models because of the above factors. Table 2 and 3 shows the mean experimental and predicted PL values obtained while Table 4 shows the indoor PL measurements in this study.

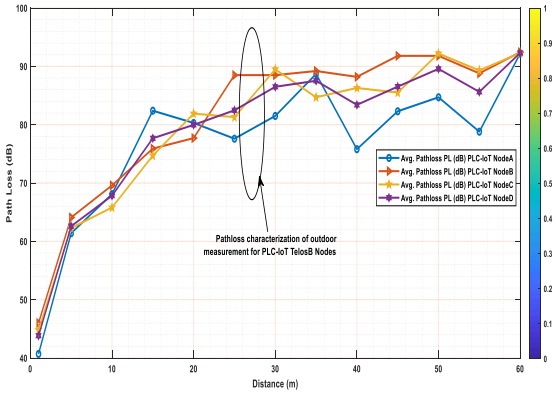

Figure 8. PL prediction with Live Nodes (L1).

Table 2. Average Experimental and predicted PL

Distance (m)	Avg. Experimental *PLm* (dB)	Avg. predicted P_{Lp} (dB)
1	43.83	43.83
5	62.60	61.96
10	67.83	70.52
15	77.67	75.32
20	79.97	78.66
25	82.47	81.34
30	86.50	83.36
35	87.53	85.15
40	83.40	86.70
45	86.53	88.06
50	89.57	89.28
55	85.63	90.39
60	92.30	91.39

Table 3. Average measured and predicted *PL*

Distance (m)	Avg. measured P_L (dB)	Avg. Predicted PL (dB)
1	44.90	44.90
2	56.53	52.94
3	63.67	57.82
4	61.50	61.28
5	62.83	63.96
6	64.73	66.15
7	62.83	68.01

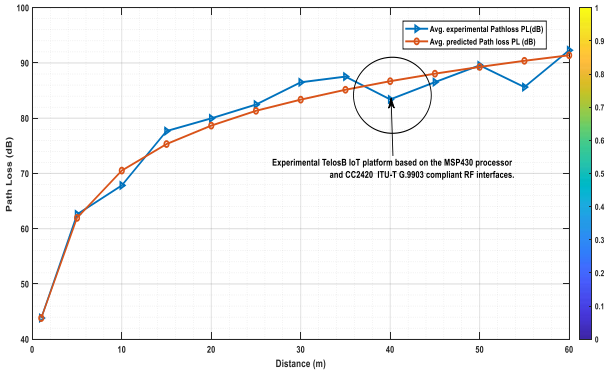

Figure 9. PL prediction Vs experimental with Live Nodes.

Table 4. Average indoor environment PL for IoT TelosB nodes.

Distance	Avg. P_L (dB) Node 1	Avg. PL (dB) Node 2	Mean P_L (dB) Node 3	Mean P_L (dB) Node 4

1	44.6	52.0	38.1	44.90
2	58.5	57.3	53.25	56.53
3	74.1	60.4	56.5	63.67
4	57.0	67.7	59.8	61.50
5	68.5	57.7	62.3	62.83
6	70.2	64.0	60.0	64.73
7	57.3	72.5	58.7	62.83

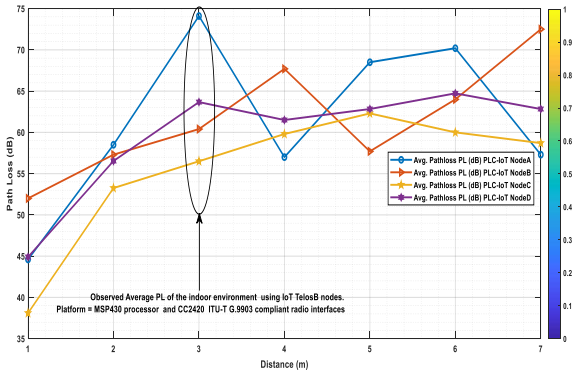

Figure 10. PL prediction with Live Nodes (L2).

B. *Energy Depletion Analysis*

The First-order radio energy dissipation model was explored in [49] and later used in other research to investigate the energy consumption pattern. E91-AA alkaline battery model and its operational characteristics were used to estimate the transceivers' battery life. The receiver uses energy to power the radio electronics, while the transmitter uses energy to run the radio electronics and power amplifier as shown in Table 5 and Table 6 respectively. Energy depletion cycles are shown in Table 6 which highlights significant energy drain during active states.

Table 5. Average Energy Depletion Cycles for IoT TelosB Nodes.

Distance	Time (min)	Battery voltage for IoT-PLC Node 1	Battery voltage of IoT-PLC Node 2	Battery voltage of IoT-PLC Node 3	Ave. Battery voltage of IoT-PLC Node 4
1	2	2.781	2.722	2.813	2.772
5	4	2.779	2.720	2.810	2.770
10	6	2.777	2.717	2.807	2.767
15	8	2.775	2.716	2.805	2.765
20	10	2.772	2.712	2.802	2.762
25	12	2.771	2.712	2.801	2.761
30	14	2.770	2.710	2.798	2.760
35	16	2.764	2.706	2.793	2.754
40	18	2.763	2.705	2.793	2.754
45	20	2.762	2.704	2.792	2.753
50	22	2.761	2.702	2.789	2.751
55	24	2.756	2.700	2.783	2.746
60	26	2.752	2.694	2.780	2.742

Table 6. Average Energy Depletion cycles for IoT TelosB nodes.

Distance	Time (min)	IoT-PLC Node 1 Depletion Rate	IoT-PLC Node 2 Depletion Rate	IoT-PLC Node 3 Depletion Rate	IoT-PLC Node 4 Depletion Rate
1	2	0	0	0	0
5	4	0.002	0.002	0.003	0.002
10	6	0.004	0.005	0.006	0.005
15	8	0.006	0.006	0.008	0.007
20	10	0.009	0.010	0.010	0.010
25	12	0.010	0.010	0.011	0.011
30	14	0.011	0.012	0.014	0.012
35	16	0.017	0.016	0.019	0.018
40	18	0.018	0.017	0.019	0.018
45	20	0.019	0.018	0.020	0.019
50	22	0.020	0.020	0.023	0.021
55	24	0.025	0.022	0.029	0.026
60	26	0.029	0.028	0.032	0.030

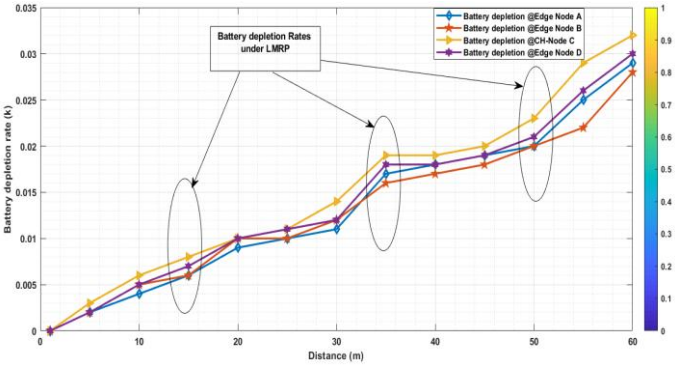

Figure 11. Energy Optimisation with Live Nodes (L2).

C. *Frequency Comparision with mmWave IoT-PLC devices*

From Figure 12, ignoring the directional antenna gain implies that mmWave IoT-PLC devices experience more severe PL than conventional Wi-Fi access point devices. IoT-PLC beamforming and directional antennas have been shown to have significantly lower PL than comparable Wi-Fi devices for short distances, though this is only true for omnidirectional antennas [48], [51]. These facts indicate that the IoT-PLC nodes that use Wi-Fi frequencies are tended to transmit messages to farther nodes, which results in more propagation loss (and a greater likelihood of message errors and a reduction in delivery ratio), while the IoT-PLC nodes using mmwave is tended to transmit messages to closer nodes and with narrow beams and high directional gains, which results in less propagation loss.

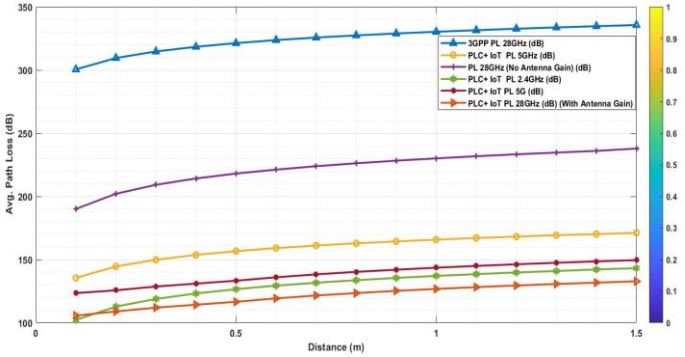

Figure 12. PL Frequency comparison.

Finally, additional effort is introduced to verify edge network scenarios and compare these scenarios. The idea is to see whether the proposed routing protocol in SPLCN performs better when utilising mmwave than when using the sub-6GHz band.

D. *Optimisation Evaluation*

In this subsection, a highly provisioned closed-loop method was adopted for data collection from the IoT network in the study areas. When deploying the optimisation algorithm for the network system, observations were recorded on a log file using the TelosB application developed in Section V-C. This was installed on the Corei3, 2.4GHz, 8G laptop. The NodeID is used to initiate different network data transmissions with testbed integration. The recorded data on the TelosB log files are later processed with excel CSV for further analysis. LMRP optimisation algorithm was then

employed to enhance the developed PL model for better performance. The PL test routes and measured data for locations L1, L2, and L3 are shown in Tables 4 and 5, respectively.

Table 6. Optimisation Transmission Parameters

Transmission Parameters	
Carrier Frequency	2.4 GHz
Data rates	250kbps
Antenna Integration	Onboard
Battery Model	2X AA batteries
Sensors	Visible light, Humidity, Temperature, Resolution, RSSI, Link indicator,
Transmission Power	43 dBm
Transmitter height	60 m
Transmitter Gain	2.0 dBi
Receiver Gain	1.8 dBi
RF Power	-24dBm to 0 dBm
Receive Sensitivity	-90 to -94 dBm
Outdoor range	75 to 100m
Indoor range	20 to 30m
Multi-path propagation	OFDM

Table 7. IoT Test locations

(Locations)	**Area in FUTO zone**
L1	Sonic Fast Food
L2	Old SEET Block
L3	SEET Complex

Using the scenarios described in Tables 3 and 4 for PL optimisation estimations, this article explored the case of one Genetic algorithm described in [30], [50] and particle optimisation [32], [34]. The PL is characterised by the dispatched IoT nodes, but the objective is to evaluate the Optimisation impact and how it could reduce losses at the edge. This is useful for Fog devices in Figure 2 during active routing operation. We assume that all the IoT Nodes within these locations are served by only one cluster head like LoRaWAN or any other LP-WAN infrastructure [36]. Each node connects the sinking facility as shown in Fig. 1. We assume the SPLCN just like the LoRaWAN network is stable. The datasets are generated uniformly distributed random variables using the MATLAB tool. The optimisation schemes are evaluated with results summarised in Table 8.

So far, a prototype edge communication network testbed based on the limited IoT MSP430 platform is discussed. It runs in an indoor setting using TelosB ITU-T G.9903 API interfaces. Fragmentation and reassembly are active at run time on the network since the maximum translation unit (MTU) for ITU-T G.9903 alongside IPv6 MTU is enabled at run time. This IoT environment incorporates PL network infrastructure capabilities. Edge-to-Fog datastream delivery and lightweight overhead were determined to be at a reasonable level using Algorithm II. The shortest path communication during routing is achieved with Algorithm I. In contrast to the previous work [47], the ITU-T G.9903 MTU permits a lower PL transmission fragmentation than in GA [30], [50] and PSO networks [32],[34], while the IEEE 802.15.4 network does not need fragmenting the signature [50]. However, TelosB's lightweight energy consumption is significantly lower than the energy consumption in most open-source hardware discussed [46], [47], [53]. This allows for longer active operational deployments even in production environments. It is important to note that the energy depletion rates during PL traffic (i.e., signal data steam) propagation remain at a low level while PL incidents under lightweight optimisation remain equally lower than other schemes. Since the software structures used are flexible and modular, the system is still up for enhancement in an ongoing container platform for driverless or connected vehicular computing.

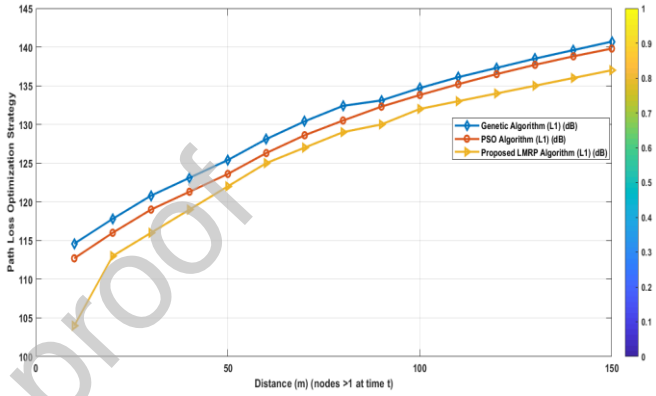

Figure 13. PL Optimisation validation with Live Nodes (L1).

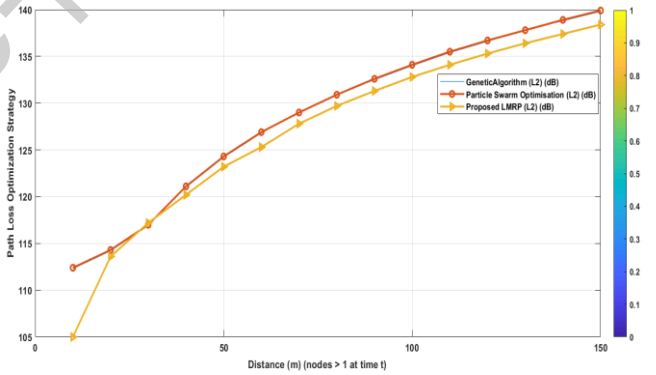

Figure 14. PL Optimisation validation with Live Nodes (L2).

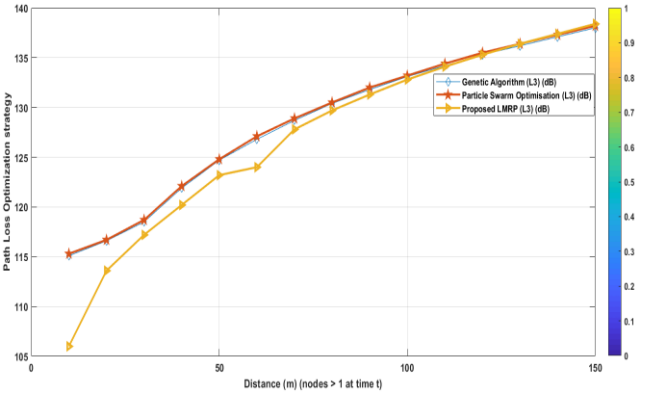

Figure 15. PL Optimisation validation with Live Nodes (L3).

Table 8. Optimisation results for live site experiments

(Locations)	**Optimisation Schemes**	**Average indicator (%)**
L1	GA	33.98
	PSO	33.25
	Proposed LMRP	**32.77**
L2	GA	33.81

	PSO	33.57
	Proposed LMRP	**32.62**
L3	GA	33.65
	PSO	33.41
	Proposed LMRP	**32.94**

At the network planning level, PL is a crucial factor in determining the quality of service (QoS) for RPL edge communication. The reason for the reduced PL from Table 8 is that we decreased the absorption losses at the deployment sights while guaranteeing minimum diffraction at the edge layers, which caused the PL to decrease. To prevent RF attenuation, the topography, buildings, and plants were all heavily managed during the routing of sensed payloads.

VI. EXPERIMENTAL VALIDATIONS

A. Comparative Analysis

In this section, the validation of the lightweight scheme for *k*-shortest path multi-hop routing from the edge to the sink location is presented. In context, clustered slave nodes (N=1000, SN_1, SN_2,…, SN_{n-1}) were built from Riverbed C++ API library. This validation used a simple master-slave network topology to assess the developed routing plan given PL incidents. The requirement for the sensing edge layer to collect data with IoT formed a PL case study. A real-time data stream is transmitted while ensuring active and reliable data stream events. The setup is provisioned for end-to-end latency and data stream offloading between nodes. The use of edge application layer protocols in various use cases is to allow for network and application layer investigations. This is optimal for end-to-end throughput and is equally needed to dynamically accelerate PL convergence. IoT lightweight protocols improve reliable real-time communications. Since the LMRP addresses routing reliability even under ITU-T G.9903 policy, we then compared the performance with earlier reviewed lightweight schemes including CoAP [20], MQTT [21], AMQP [22], XMPP [23] and RESTful-API [24]. In this case, to determine the impact of the proposed LMRP, an application layer comparison is made considering minimal PL incidents. The validation study considered data stream latency, end-to-end reliability, and computational complexity. The edge communication network is then tested for distributed lightweight routing decisions. For simplicity, the proposed lightweight resource allocation policy is verified with the network nodes accommodated at the edge clusters in subnets. To make it easier to route sensed data to the sink, we spaced the sensor nodes 20 meters apart and added a cluster head (CH) every 40 meters. A bandwidth of 200 Mbit/s to 1.5Gbit/s, 50 ms max latency, and 200m max transmission distance is enabled. Initially, each upstream node generates sensed data using the proposed LMRP technique. This sends the information to the subsequent cluster head, which then passes it to a sink. Each sensor transmits a maximum of 1500 datastream (or translation units) to the CH in a multi-fashion manner. The selected metrics are discussed below.

B. Throughput dynamics

After parameter configurations with G.9903, the throughput model based on CQARPL [18] is used to validate the LMRP method considering the edge-to-Fog PLC network. In this case, similar lightweight algorithms such as REST, CoAP, and MQTT were compared with the proposed scheme. The idea is to enhance edge computing dependability in a production IoT-PLC deployment. Recall that the application layer is the interface between edge nodes and the Fog network communication. It manages datastream presentation, and formatting and acts as a link between what a node is doing and how the data it generates is transferred across a network. It is shown that the datastream throughput from the edge cluster to the application layer is consistent and optimal at 43.47% as detailed in Table 9. This implies that the routing capabilities for IoT-enabled services are fully optimised, unlike REST, CoAP, and MQTT which had 8.70%, 26.09%, and 21.74% respectively. Another way of looking at Figure 16 is that it demonstrates the impact of varied edge-node density in the context of network permeability. Even though the throughput increases as the number of nodes do, yet the results reveal that LMRP performed better with additional nodes. This illustrates that the proposed scheme had greater success with improved QoS routing capacity.

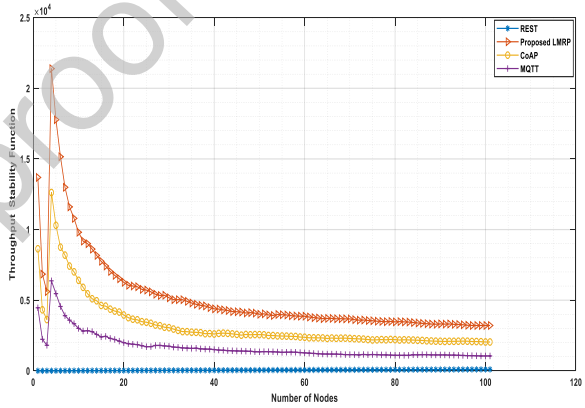

Figure16: Edge-to-Fog throughput comparison with node increments.

C. Delay Provisioning (Latency Phase)

The delay in the raising phase seen in Figure 17 is because of the payload overhead which introduces inherent propagation convergence latency before the transmission upstream phase. This study reveals convergence time through network latency whenever a new node is added or removed. This converges within a few seconds due to the lightweight routing provisioning at the edge. If a node is re-established or loses connectivity, it must converge within 0.2 seconds which is better than RPL [1], CQARPL [18], and CLRPL [54]. Also, if no nodes have dropped in its subnet location, the convergence becomes much smaller < 0.2s. This leads to lower CPU and memory utilisation cycles when considering computational complexity. Therefore, end-to-end latency is used to validate the convergence time for data stream propagation considering CoAP, MQTT, AMQP, XMPP, and REST via node synchronous request-response in Table 10. Because increasing the datastream traffic rate leads to channel congestion, this directly affects edge network traffic. Nonetheless, LMRP experiences less latency (at least 3.04%) than the other protocols as the traffic rate rises. This suggests better LMRP performance with more data stream traffic and optimal PL. This could be used to forecast impulsive congestion and direct traffic along the shortest least-congested routes.

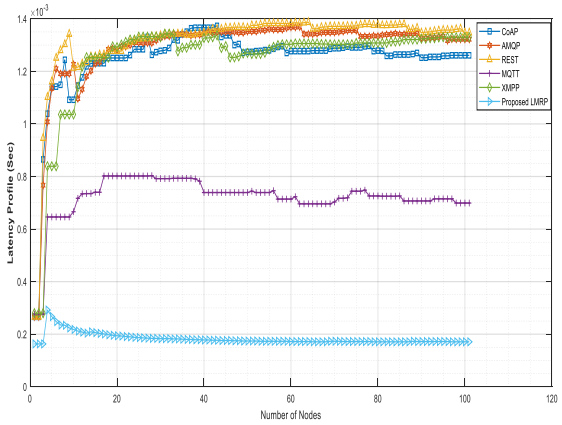

Fig. 17. Edge-to-Fog latency provisioning with node increments.

From Figure 18, the minimum overhead with lightweight routing under impulsive noise is 16.67% compared with similar lightweight protocols like CoAP and MQTT having 37.04% and 46.29% respectively in Table 11. Every IoT-PLC node is linked to the edge grid network with inherent impulsive noise. With Middleton's class *A* model [54], and LMRP optimisation strategy, the noise is reduced by at least 16.67%. As shown in the plot, the dropping of the peak noise spikes is useful. The Middleton's class *A* median filter reduces remove impulse noise. Hence, the proposed scheme equally serves as an impulse noise filter. This improves the robustness of the edge network channel. A practical application is in adaptive control and IoT pattern recognition systems.

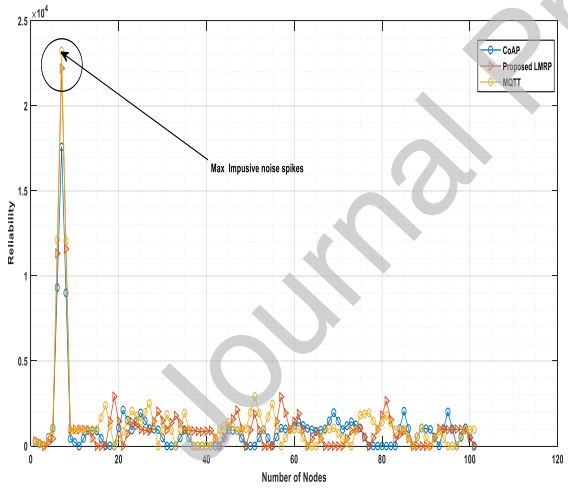

Figure 18: Edge-to-Fog reliability overhead with node increments.

For the established edge communication network to maintain stability, dynamic reliability is needed to make both node integration and routing possible. Network adjacencies must use the RPL to harvest link states in nearby nodes. Each full-duplex path in the edge network must avoid routing loops. The implication of the SPLCN architecture under the proposed routing scheme is that transactional provisioning of the datastream workload is guaranteed.

D. Computational Complexity

Figure 19 shows the computational complexity of a recurrence linear search algorithm $T(N) = T(N-1) + 0(1) = O(N)$. The Big-O is active when considering the failure density rate/stability at the edge cluster. MCFP optimisation technique in Section III-C alongside the node distributed control is very significant and makes the LMRP algorithm I and II attractive under ITU-T G.9903. It can support enterprise-scaled deployments compared to existing lightweight algorithms. It is shown that with an autoscaling algorithm in edge-to-Fog layered orchestration (as depicted in Algorithm I). The performance response for the proposed scheme (LMRP), generic RPL [1], and CQARPL [18] are 8.98%, 41.07%, and 50.0%, respectively, in Table 12. This result shows that minimum time-space complexity is favorable for LMRP in terms of read-read input datasets.

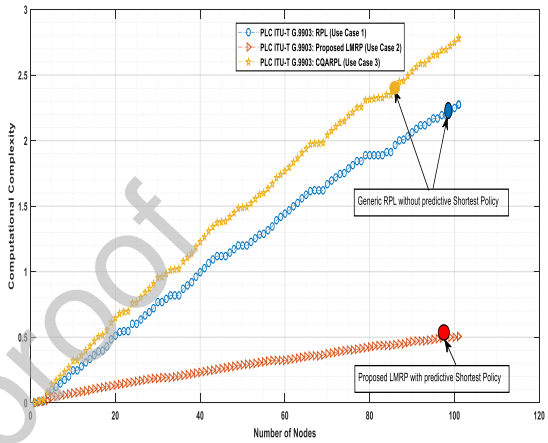

Figure 19: Edge-to-Fog computational complexity function comparisons.

With lower computational complexity, this will reinforce the confidence of the layered optimisation supports even under other edge resources like the smart power pool for IoT-PLC edge nodes. Again, the usefulness of the MCFP formulation is that the edge clusters gain more stability leading to better performance. Finally, the lightweight link-design for edge networks enhances the overall performance of the SPLCN architecture. Computational offloading in SPLCN solves latency problems during routing and optimises PL. Uniform workload distribution at the edge-to-Fog layers compensates for cascaded subnet clusters at the edge. This notwithstanding, more efforts are needed to consolidate access control such as [56], [57].

Table 9. Result summary of Edge network Throughput metric

Lightweight IoT Schemes	**Throughput (Bytes/sec)**
REST [24]	8.70%
CoAP [20]	26.90%
MQTT [21]	21.74%
Proposed LMRP	43.47%

Table 10. Result summary of Edge network latency metric

Routing Schemes	**Latency Profile (Secs)**
CoAP [20]	19.74%
AMQP [22]	21.37%
REST [24]	22.51%
MQTT [21]	13.05%
XAMPP [23]	20.06%
Proposed LMRP	3.04%

Table 11. Result summary of Edge network reliability

Routing Schemes	**Reliability**
CoAP [20]	37.04%
MQTT [21]	46.29%
Proposed LMRP	16.67%

Table 12. Result summary of computational complexity metric.

Routing Schemes	Computational Complexity
RPL [1]	41.07%
CQARPL [54]	50.00%
Proposed LMRP	8.93%

VII. CONCLUSION

In this article, a layered full-duplex IoT-PLC edge network architecture is proposed for supporting lightweight Multi-hop RPL. For edge devices connected to the network, we showed the deployment distribution as a directed graph and highlighted the minimum cost flow problem formulation (MCFPF). Algorithms for the shortest path and lightweight connection policy are presented. Practical path loss and radio energy models were derived and demonstrated to illustrate edge network deployment context. Path loss mitigation and energy depletion of classical TelosB nodes further presented edge computing characteristics. With the proposed LMRP scheme, better PL and routing optimisation responses are achieved. Similarly, when subjected to ITU-T G.9903, LMRP performed better than RESTful API, CoAP, MQTT, XMPP, and AMQP on four (4) major metrics related to IoT-PLC applications. The application of lightweight protocols can be used to reduce complex channel traffic density and enhance the lifespan of IoT-PLC setups. The proposed algorithm can be applied to minimise computational overhead on connection-oriented edge interfaces such as smart grids and driverless cars. However, the proposed method did not consider other complex edge computing network features and parameters. Future work will improve the proposed lightweight method and deploy it in containerised driverless cars as a use case. Also, edge analytics using lightweight spike neural network data stream processing will be addressed.

Funding: "This work was supported by Tetfund Nigeria under Grant "TETF/ES/UNIV/IMO STATE/TSAS/2021". (Ref Project: Cyberphysical driverless Car with Resilient AI).

References

[1] R. -G. Tsai, P. -H. Tsai, G. -R. Shih and J. Tu, "RPL Based Emergency Routing Protocol for Smart Buildings," in *IEEE Access*, vol. 10, pp. 18445-18455, 2022.

[2] R. Onoshakpor, K. C. Okafor and M. Gabriel, "Smart Grid Reliability Computation - A Solution to Ageing Infrastructure in Power Grid Networks," *IEEE Nigeria 4th Int'l Conf on Disruptive Tech for Sustainable Dev (NIGERCON)*, Lagos, Nigeria, 2022, pp. 1-5.

[3] J. Zhao, X. Chang, Y. Feng, C. H. Liu, and N. Liu, "Participant Selection for Federated Learning with Heterogeneous Data in Intelligent Transport System," *in IEEE Transactions on Intelligent Transportation Systems*, 24(1), pp. 1106-1115, 2023.

[4] H. -S. Kim, J. Ko, D. E. Culler, and J. Paek, "Challenging the IPv6 Routing Protocol for Low-Power and Lossy Networks (RPL): A Survey," *in IEEE Communications Surveys & Tutorials*, 19(4), pp. 2502-2525, Fourthquarter 2017.

[5] Safara, F., Souri, A., Baker, T. et al. PriNergy: a priority-based energy-efficient routing method for IoT systems. J Supercomput 76, 8609–8626, 2020.

[6] K. C. Okafor, M. C. Ndinechi, Sanjay Misra, "Cyber-Physical Network Architecture for Smart City Data Stream Provisioning in Complex Ecosystems", *In Transactions on Emerging Telecommunications Technologies*, 32(11), Pp.1-31, 2021.

[7] V. Korzhun and A. M. Tonello, "Channel Tracking for Future Powerline-based Full-Duplex Smart Grid Communication Networks, *"Int'l Conf. on Smart Sys. and Tech (SST),* Osijek, Croatia, 2022, pp. 87-92.

[8] G. Prasad, L. Lampe and S. Shekhar, "Enhancing transmission efficiency of broadband plc systems with in-band full duplexing", *Int'l Symp. on Power Line Comm. and its Appl. (ISPLC)*, pp. 46-51, 2016.

[9] Zhou, L., Xiao, L., Yang, Z. *et al*. "Path loss model based on cluster at 28 GHz in the indoor and outdoor environments". *Sci. China Inf.* Sci. 60, 080302, 2017.

[10] B. De Beelde, E. Tanghe, M. Yusuf, D. Plets and W. Joseph, "Radio Channel Modeling in a Ship Hull: Path Loss at 868 MHz and 2.4, 5.25, and 60 GHz," *in IEEE Antennas and Wireless Propagation Letters*, 20(4), pp. 597-601, 2021.

[11] W. Hong *et al.*, "The Role of Millimeter-Wave Technologies in 5G/6G Wireless Communications," *in IEEE Journal of Microwaves*, 1(1), pp. 101-122, 2021.

[12] T. Okuyama, S. Suyama, N. Nonaka, Y. Okumura and T. Asai, "Outdoor Experimental Trials of Millimeter-Wave Base Station Cooperation with Digital Beamforming in High-Mobility Environments for 5G Evolution," *IEEE 92nd Vehicular Tech. Conf. (VTC2020-Fall)*, Victoria, BC, Canada, 2020, pp. 1-5.

[13] L. Zheng, W. Chen and Y. Tian, "Edge-Computing Oriented Robust Routing Scheme in IoT-PLC Networks, "*IEEE 5th Int'l Conf on Elect. Tech (ICET)*, Chengdu, China, 2022, pp. 994-997.

[14] H. Kim, H. -S. Kim and S. Bahk, "MobiRPL: Adaptive, robust, and RSSI-based mobile routing in low power and lossy networks," *in Journal of Communications and Networks*, 24(3), pp. 365-383, 2022.

[15] B. Ghaleb *et al.*, "A Survey of Limitations and Enhancements of the IPv6 Routing Protocol for Low-Power and Lossy Networks: A Focus on Core Operations," in IEEE Communications Surveys & Tutorials, vol. 21, no. 2, pp. 1607-1635, Secondquarter 2019,

[16] Y. Kim and J. Paek, "NG-RPL for Efficient P2P Routing in Low-Power Multi-hop Wireless Networks," *in IEEE Access*, vol. 8, pp. 182591-182599, 2020.

[17] Safara, F., Souri, A., Baker, T. *et al*. "PriNergy: a priority-based energy-efficient routing method for IoT systems". *J Supercomput* 76, 8609–8626, 2020.

[18] Kaviani, F., Soltanaghaei, M. CQARPL: Congestion and QoS-aware RPL for IoT applications under heavy traffic. *J Supercomput* 78, 16136–16166, 2022.

[19] S. -T. Liu and S. -D. Wang, "Improved Trickle Algorithm Toward Low Power and Better Route for the RPL Routing Protocol," *in IEEE Access*, vol. 10, pp. 83322-83335, 2022.

[20] F. Righetti, C. Vallati, D. Rasla and G. Anastasi, "Investigating the CoAP Congestion Control Strategies for 6TiSCH-Based IoT Networks," *in IEEE Access*, vol. 11, pp. 11054-11065, 2023.

[21] M. Hamad, A. Finkenzeller, H. Liu, J. Lauinger, V. Prevelakis and S. Steinhorst, "SEEMQTT: Secure End-to-End MQTT-Based Communication for Mobile IoT Systems Using Secret Sharing and Trust Delegation," *in IEEE Internet of Things J*, 10(4), pp. 3384-3406, 15 Feb.15, 2023.

[22] D. Yoshino, Y. Watanobe and K. Naruse, "A Highly Reliable Communication System for Internet of Robotic Things and Implementation in RT-Middleware with AMQP Communication Interfaces," *in IEEE Access*, vol. 9, pp. 167229-167241, 2021.

[23] H. Wang, D. Xiong, P. Wang and Y. Liu, "A Lightweight XMPP Publish/Subscribe Scheme for Resource-Constrained IoT Devices," *in IEEE Access*, vol. 5, pp. 16393-16405, 2017.

[24] "IEEE Draft Standard for Learning Technology - JavaScript Object Notation (JSON) Data Model Format and Representational State Transfer (RESTful) Web Service for Learner Experience Data Tracking and Access," *in IEEE P9274.1.1/D4.0*, pp.1-155, 6 Feb. 2023.

[25] C. Li, Y. Liu, J. Xiao, and J. Zhou, "MCEAACO-QSRP: A Novel QoS-Secure Routing Protocol for Industrial Internet of Things," *in IEEE Internet of Things J.*, 9,(19), pp. 18760-18777, 1, 2022

[26] H. Yan, Y. Xie, X. Yang and T. Song, "A Novel Algorithm for Reducing the Power Loss of Routing Paths in ONoCs," 2020 *Int'l Conf., on Wireless Comm. and Signal Proc (WCSP),* Nanjing, China, 2020, pp. 325-330.

[27] L. Wu *et al.*, "Artificial Neural Network Based Path Loss Prediction for Wireless Communication Network," *in IEEE Access*, vol. 8, pp. 199523-199538, 2020.

[28] G. M. Bianco, R. Giuliano, F. Mazzenga and G. Marrocco, "Multi-Slope Path Loss and Position Estimation with Grid Search and Experimental Results," *in IEEE Trans on Signal and*

Information Processing over Networks, vol. 7, pp. 551-561, 2021.
[29] G. -J. Jong, Z. -H. Wang, Hendrick, K. -S. Hsieh and G. -J. Horng, "A Novel Adaptive Optimisation of Integrated Network Topology and Transmission Path for IoT System," *in IEEE Sensors J*, 19(15), pp. 6452-6459, 2019.
[30] Y. Pan, Y. Yang and W. Li, "A Deep Learning Trained by Genetic Algorithm to Improve the Efficiency of Path Planning for Data Collection with Multi-UAV," *in IEEE Access*, vol. 9, pp. 7994-8005, 2021.
[31] T. Sefako and T. Walingo, "Biological Resource Allocation Algorithms for Heterogeneous Uplink PD-SCMA NOMA Networks," *in IEEE Access*, vol. 8, pp. 194950-194963, 2020,
[32] A. A. Nagra, F. Han, Q. -H. Ling and S. Mehta, "An Improved Hybrid Method Combining Gravitational Search Algorithm with Dynamic Multi Swarm Particle Swarm Optimisation," *in IEEE Access*, vol. 7, pp. 50388-50399, 2019.
[33] H. Wen, Y. Lin and J. Wu, "Co-Evolutionary Optimisation Algorithm Based on the Future Traffic Environment for Emergency Rescue Path Planning," *in IEEE Access*, vol. 8, pp. 148125-148135, 2020.
[34] H. M. Jawad *et al.*, "Accurate Empirical Path-Loss Model Based on Particle Swarm Optimisation for Wireless Sensor Networks in Smart Agriculture," *in IEEE Sensors J*, 20(1), pp. 552-561, 2020.
[35] D. D. Lieira, M. S. Quessada, A. L. Cristiani, R. Immich and R. I. Meneguette, "TRIAD: Whale Optimisation Algorithm for 5G-IoT Resource Allocation Decision in Edge Computing," 1*6th Iberian Conf on Inf. Sys & Tech (CISTI)*, Portugal, 2021, pp. 1-6.
[36] S. Lukman, Y. Y. Nazaruddin, B. Ai and E. Joelianto, "The New Empirical Path Loss Model for Line-of-Sight Propagation in HSR Communication System Using Optimisation Technique," *in IEEE Wireless Comm. Letters*, 11(9), pp. 1810-1814, Sept. 2022.
[37] D. Casillas-Pérez, D. Merino-Pérez, S. Jiménez-Fernández, J. A. Portilla-Figueras and S. Salcedo-Sanz, "Extended Weighted ABG: A Robust Non-Linear ABG-Based Approach for Optimal Combination of ABG Path-Loss Propagation Models," *in IEEE Access*, vol. 10, pp. 75219-75233, 2022.
[38] W. Tang *et al.*, "Path Loss Modeling and Measurements for Reconfigurable Intelligent Surfaces in the Millimeter-Wave Frequency Band," *in IEEE Trans on Comm*, 70(9), pp. 6259-6276, 2022.
[39] Y. Yoon and H. J. Park, "Excess Loss by Urban Building Shadowing and Empirical Slant Path Model," *in IEEE Antennas and Wireless Prop., Letters*, 21(2), pp. 237-241, 2022.
[40] L. Wu *et al.*, "Artificial Neural Network Based Path Loss Prediction for Wireless Communication Network," *in IEEE Access*, vol. 8, pp. 199523-199538, 2020.
[41] B. Adebisi, K. Anoh, K. M. Rabie, A. Ikpehai, M. Fernando and A. Wells, "A New Approach to Peak Threshold Estimation for Impulsive Noise Reduction Over Power Line Fading Channels," *in IEEE Systems Journal*, 13(2), pp. 1682-1693, 2019.
[42] W. Mei and R. Zhang, "Multi-Beam Multi-Hop Routing for Intelligent Reflecting Surfaces Aided Massive MIMO," *in IEEE Trans on Wireless Comm*, 21(3), pp. 1897-1912, 2022.
[43] M. Pióro and D. Medhi, Routing Flow and Capacity Design in Communication and Computer Networks—*A Volume in the Morgan kaufmann Series in Networking*, Amsterdam, The Netherlands: Elsevier, 2004.
[44] T. Mahmood, W. Q. Mohamed and O. A. Imran, "Factors Influencing the Shadow Path Loss Model with Different Antenna Gains Over Large-Scale Fading Channel," *Int'l Conf on Artificial Intell. and Mech. Sys.,(AIMS)*, Indonesia, pp. 1-5, 2021.
[45] TelosB Mote Platform. Available Online: *https://www.willow.co.uk/TelosB_Datasheet.pdf*
[46] C. P. Quitevis and C. D. Ambatali, "Feasibility of an Amateur Radio Transmitter Implementation Using Raspberry Pi for a Low Cost and Portable Emergency Communications Device," *IEEE Global Humanitarian Tech. Conf (GHTC)*, San Jose, CA, USA, 2018, pp. 1-6.
[47] K. C. Okafor, Omowunmi Mary Longe, "Smart deployment of IoT-TelosB service care StreamRobot using software-defined reliability optimisation design, *Heliyon*, 8(6), 2022.
[48] M. Amjad, M. Sharif, M. K. Afzal and S. W. Kim, "TinyOS-New Trends, Comparative Views, and Supported Sensing Applications: A Review," *in IEEE Sensors J*. 16(9), pp. 2865-2889, 2016.
[49] A. Ikpehai *et al*., "Low-Power Wide Area Network Technologies for Internet-of-Things: A Comparative Review," in *IEEE Internet of Things Journal*, 6(2), pp. 2225-2240, 2019.
[50] B. -h. Lee, D. Ham, J. Choi, S. -C. Kim and Y. -H. Kim, "Genetic Algorithm for Path Loss Model Selection in Signal Strength-Based Indoor Localization," *in IEEE Sensors Journal*, 21(21), pp. 24285-24296, 1 Nov.1, 2021.
[51] N. K. Maurya, M. J. Ammann and P. Mcevoy, "Series-Fed Omnidirectional mm-Wave Dipole Array," *in IEEE Transactions on Antennas and Propagation*, 71(2), pp. 1330-1336, Feb. 2023.
[52] S. -Y. Ooi, P. -S. Chee, E. -H. Lim, J. -H. Low and F. -L. Bong, "A Zeroth-Order Slot-Loaded Cap-Shaped Patch Antenna with Omnidirectional Radiation Characteristic for UHF RFID Tag Design," *in IEEE Transactions on Antennas and Propagation*, vol. 71(1), pp. 131-139, 2023.
[53] E. Schiller, E. Esati, S. R. Niya and B. Stiller, "Blockchain on MSP430 with IEEE *802*.15.4," *IEEE 45th Conf. on Local Computer Networks (LCN)*, Sydney, NSW, Australia, 2020, pp. 345-348.
[54] S. Taghizadeh, H. Bobarshad and H. Elbiaze, "CLRPL: Context-Aware and Load Balancing RPL for IoT Networks Under Heavy and Highly Dynamic Load," *in IEEE Access*, vol. 6, pp. 23277-23291, 2018.
[55] A. Van Laere, S. Bette and V. Moeyaert, "Poster: ITU-T G.9903 performance against Middleton class-A impulsive noise," *Symp. on Comm. and Vehicular Tech (SCVT)*, Mons, Belgium, 2016, pp. 1-6.

Dear Editor

I have the pleasure of sending you our manuscript entitled "***Compact Computational Model for Market Place Service Robot: A Novel Parameterization for identifying and Controlling COVID-19 infection Transmission Dynamics"*** to be considered for publication as a research article in your prestigious Journal. This paper covers a novel effort in building resilient health infrastructure for global vaccination as well as tackling the COVID-19 variants of interest. Novel computational models were developed while verifying their computational complexities.

All authors have seen and approved the manuscript and have contributed significantly to the paper.

Ethical Procedure

* The research meets all applicable standards concerning the ethics of experimentation and research integrity, and the following is being certified/declared true.

* As an expert scientist and along with co-authors of the concerned field, the paper has been submitted with full responsibility, following the due ethical procedure, and there is no duplicate publication, fraud, plagiarism, or concerns about animal or human experimentation.

A DISCLOSURE / CONFLICT OF INTEREST STATEMENT

* None of the authors of this paper has a financial or personal relationship with other people or organizations that could inappropriately influence or bias the content of the paper.

* It is to specifically state that "No Competing interests are at stake and there is No Conflict of Interest" with other people or organizations that could inappropriately influence or bias the content of the paper.

Corresponding Author: Dr. Kennedy Chinedu Okafor, Senior Member IEEE
Affiliation: Federal University of Technology Owerri, Nigeria
E-mail: k.okafor@mmu.ac.uk, kennedy.okafor@futo,edu.ng; kennedy.okafor@ieee.org
Phone: +2348034180668